Associative ionization between two laser-excited sodium atoms: Theory compared to experiment

Boichanh Huynh, Olivier Dulieu, and Françoise Masnou-Seeuws
Laboratoire Aimé Cotton, Bâtiment 505, Campus d'Orsay, 91405 Orsay Cedex, France
(Received 18 February 1997)

A theoretical model for the reaction $Na(3p)+Na(3p)\rightarrow Na_2^{+}+e$ is compared to a large number of experimental data. This model is considering population of long-range adiabatic Na_2 molecular states from two colliding excited atoms, and transfer of this population to short-range doubly excited autoionizing states of $^3\Sigma_u^+$, $^1\Sigma_g^+$, $^3\Pi_u$, $^1\Pi_u$, $^1\Delta_g$, and $^3\Delta_u$ symmetries. Good agreement is obtained with experimental results for total cross sections and polarization dependence of the ion signal at collision velocities $v_c \geqslant 400$ m/s. At lower velocities the sudden approximation for spin uncoupling is not valid. The computed velocity dependence of the ion signal does not reproduce the maximum in the ion signal observed in some experiments.
[S1050-2947(98)02401-9]

PACS number(s): 34.50.Rk, 33.80.Eh

I. INTRODUCTION

Associative ionization (AI) between two laser-excited alkali atoms has been the subject of much experimental investigations in the 1980s, as was reviewed in Ref. [1]. The prototype reaction was

$$Na(3p)+Na(3p)+\varepsilon \rightarrow Na_2^{+}+e+\varepsilon', \tag{1}$$

for which much data are available at thermal collision energies ε, including rate constants measured in cell experiments [2], studies of velocity or polarization dependence of the cross sections, mainly by the Utrecht [3–5] and the Maryland [6–10] groups, and analysis of the vibrational state population of the final ion by electron spectroscopy [11] or photodissociation [12,13]. This reaction therefore appears as a benchmark for theoretical methods dealing with associative ionization. Process (1) is interesting because it is a simple example of the formation of a chemical bond, and because polarization of the exciting light can be used to control the reaction.

For a long time, if qualitative theoretical models could be developed [14–16], a full quantitative treatment was not possible. Indeed, reaction (1) can be considered as a three-step process. At large internuclear distances, the first step consists of population sharing between several adiabatic molecular states, starting from a given preparation of the colliding atoms in particular Zeeman sublevels:

$$Na(3p;{}^2P_{j_A m_A})+Na(3p;{}^2P_{j_B m_B})+\varepsilon \rightarrow Na_2(\mathcal{A}n^{2S+1}\Lambda_{g/u})+\varepsilon. \tag{2}$$

The initial state of reaction (2) depends upon the excitation scheme: the polarization of the exciting light, and the geometry of the experiment. In the following it will be either $Na(3p)+Na(3p)$ or a particular combination of fine structure levels (j_A, $j_B=\frac{3}{2},\frac{3}{2}$; $\frac{3}{2},\frac{1}{2}$; $\frac{1}{2},\frac{1}{2}$.) A sudden approximation is generally used to estimate the population of a molecular state from two separated atoms [14,15]. In Eq. (2), the molecular electronic state $\mathcal{A}n^{2S+1}\Lambda_{g/u}$, which has been populated, is the nth adiabatic state in Hund's case-a representation (spin S, projection of the electronic total orbital momentum Λ, gerade/ungerade symmetry).

At intermediate distances $R\approx 10-13a_0$ ($1a_0\approx 0.053$ nm), there is formation of a Rydberg quasimolecule, and population of the pth doubly excited diabatic state of the same symmetry, denoted by $\mathcal{D}p^{2S+1}\Lambda_{g/u}$:

$$Na_2(\mathcal{A}n^{2S+1}\Lambda_{g/u})+\varepsilon \rightarrow Na_2{}^{**}(\mathcal{D}p^{2S+1}\Lambda_{g/u})+\varepsilon. \tag{3}$$

This second step is the missing link in most treatments, which assume direct population of a doubly excited $\mathcal{D}p^{2S+1}\Lambda_{g/u}$ from the two separated atoms. At small internuclear distances, $R<10a_0$, the autoionization of this doubly-excited state occurs as the third step, leaving a molecular ion in a rovibrational state (v^+, J^+):

$$Na_2{}^{**}(\mathcal{D}p^{2S+1}\Lambda_{g/u})+\varepsilon \rightarrow Na_2{}^{+}(v^+,J^+)+e+\varepsilon'. \tag{4}$$

The difficulty of the treatment lies within the combination of these three steps in the theoretical model, as well as in the large number of potential curves that are involved.

Ten molecular symmetries are likely to be populated [1] through reactions (2) and (3), and may contribute to reaction (4): for each of these channels, the population process is different, so that one may expect that the dependence of the ion signal upon the polarization of the exciting laser light, for a given geometry of the experiment, is a signature of the channels which contribute to Eq. (4). In such an interpretation, one neglects rotational coupling. The various diabatic doubly excited curves were computed for the first time in Ref. [17] and a multichannel quantum defect treatment (MQDT) of the molecular autoionization reaction (4) was proposed in Ref. [18]. A given doubly excited state will contribute, provided that the corresponding potential curve does cross the $Na_2{}^{+}$ potential curve $\mathscr{E}_0(R)$ in the vicinity of the minimum, or at least at a distance R_X such that reaction (4) is energetically possible. A qualitative agreement was obtained with one experiment [3] using linearly polarized light to excite colliding atoms from two counterpropagating beams, and measuring the dependence upon the angle between the polarization vector and the atomic beam: assuming direct population of the doubly excited state from separated atoms,

reaction (4) seemed to be dominated by the $\mathcal{D}2\,^3\Sigma_u^+$ channel. However, more accurate model potential calculations were next performed [19], and the doubly excited curves deduced from such calculations [20] suggested that four or five doubly excited states of different symmetries could contribute to the molecular autoionization process: for some of them, in particular the $\mathcal{D}1\,^3\Pi_u$ state, the dependence of the population upon the excitation scheme markedly differs from that of the $\mathcal{D}2\,^3\Sigma_u^+$ channel. Surprisingly enough, this conclusion did not modify significantly the previous theoretical predictions for polarization dependence of the ion signal. Indeed, besides a modified description of the autoionization reaction (4), the theoretical model now incorporates intermediate range dynamics [reaction (3)], showing a population sharing between various adiabatic curves correlated to dissociation limits differing from $\mathrm{Na}(3p)+\mathrm{Na}(3p)$ [for instance, $\mathrm{Na}(3s)+\mathrm{Na}(4d,5s)$], and allowing for a loss of flux, in particular in the $\mathcal{D}1\,^3\Pi_u$ channel. For the first time, quantitative predictions were proposed for the total cross sections as a function of ε in the 1–180-meV energy range. It therefore seems worthwhile to revisit the interpretation of the various experiments in the light of those new theoretical results. In particular, analysis of the energy dependence of the results could manifest the presence of thresholds for reaction (4): the opening of the $\mathcal{D}1\,^3\Delta_u$ ionization channel, predicted by the theory for a collision energy around 70 meV, should be manifested in the experimental results.

Besides its intrinsic interest, reaction (1) has been widely used in the recently opened field of cold atom collisions. Photoassociation spectroscopy with ion detection [21–24] is currently using a very similar scheme: a two-photon excitation of a pair of colliding atoms in their ground state is populating very high-lying rovibrational levels $(v_f,\ J_f)$ of the long-range molecular state Ω correlated to the $3s+3p$ limit, so that reaction (2) is replaced by reactions (5) and (6):

$$\mathrm{Na}(3s)+\mathrm{Na}(3s)+h\nu_1\rightarrow \mathrm{Na}_2(3s,3p,\Omega;v_i,J_i), \qquad (5)$$

$$\mathrm{Na}_2(3s3p,\Omega;v_i,J_i)+h\nu_2 \rightarrow \mathrm{Na}_2{}^{**}([\mathcal{A}n^{2S+1}\Lambda_{g/u}\rightarrow\mathcal{D}p^{2S+1}\Lambda_{g/u}];v_f,J_f). \qquad (6)$$

Such a process is usually referred to as photoassociative ionization. The frequency ν_1 of the first photon is redshifted from the atomic resonance line in view of populating a loosely bound level of the dimer. The frequency ν_2 of the second photon is varied around ν_1. In Eq. (6), our model predicts the population of molecular states which are adiabatic at long range and diabatic at short range. Those states therefore have two labellings for a given symmetry; p at short range, and n at long range.

Reaction (4) is now changed into Eq. (7),

$$\mathrm{Na}_2{}^{**}(\mathcal{D}p^{2S+1}\Lambda_{g/u};v_f,J_f)\rightarrow \mathrm{Na}_2{}^{+}(v^+,J^+)+e+\varepsilon'. \qquad (7)$$

The long-range part of the interatomic potentials could be accurately checked by photoassociation experiments on the condition that doubly excited states can be populated and *do produce an ion signal* or an *electron signal*. A revival of interest is rising for the knowledge of those doubly excited states and their autoionization efficiency: the existence of a possible threshold for reaction (7) is of particular interest for the interpretation of existing experiments [24] or for the definition of new ones.

In Refs. [24, 25], a nuclear continuum level is also populated in the second step, reaction (6) now being:

$$\mathrm{Na}_2(3s3p,\Omega;v_i,J_i)+h\nu_2\rightarrow \mathrm{Na}_2(\mathcal{A}n^{2S+1}\Lambda_{g/u})+\varepsilon, \qquad (8)$$

so that the associative ionization is studied at ultracold collision energies ε.

The aim of the present paper is therefore to check for the validity and limitations of the theoretical model of Ref. [20] by comparing the computed cross sections to a large number of significant experimental results corresponding to various excitation schemes and collision energies in the thermal domain. This model is summarized in Sec. II, and new results for the molecular autoionization through a $^3\Delta_u$ channel are incorporated. In order to compare with experimental data, the cross sections corresponding to the different channels first have to be combined to take account of the initial state in Eq. (2) created through a given choice of polarization of the exciting lasers; then, convolution with velocity distribution must be performed. Different experiments are briefly described in Sec. III, where reaction (1) is analyzed either in a cell or in beams, and the corresponding theoretical prediction for the ion signal is computed. In the present work, we do not consider experiments where the rovibrational state of the product ion is analyzed. A detailed comparison is performed in Sec. IV, insisting on the signature of the contribution of the $^3\Pi_u$ and $^3\Delta_u$ channels as cross-checked by various experiments. Finally, Sec. V discusses the extrapolation to cold collisions. Atomic units will be used except when otherwise stated.

II. THEORETICAL MODEL

Accurate model potential calculations for the excited electronic states of the Na_2 molecule have been found to be in very good agreement both with pseudopotential calculations and with experiment [19]. Such calculations do not introduce fine-structure coupling. The molecule is described as two electrons moving in the field of two polarizable cores; the electron-core interaction is represented by a model potential [26] with three adjustable parameters fitted on an atomic spectrum. Core-polarization corrections are introduced, which contain a fourth semiempirical parameter. The $Na_2{}^+$ problem is first solved on a wide range of internuclear distances, providing accurate determination of the 50σ, 38π, and 28δ lowest orbitals of the molecular ion. Adiabatic potential curves are obtained by diagonalization of the two-electron Hamiltonian in the full space of two-electron configurations constructed from the $Na_2{}^+$ orbitals. In contrast, as discussed in Ref. [20], diabatic potential curves can be obtained for a given symmetry i by partition of the configuration space into two subspaces $\mathcal{P}_i$ and $\mathcal{Q}_i$. Singly and doubly excited Rydberg series of molecular states are obtained by (i) building the $\mathcal{P}_i$ subspace by considering, for each symmetry, all singly excited configurations, for which one electron occupies the ground state orbital of $Na_2{}^+$ and the other one any $Na_2{}^+$ orbital; (ii) diagonalizing the Hamiltonian within the full subspace $\mathcal{P}_i$ yielding singly excited Rydberg series; (iii)

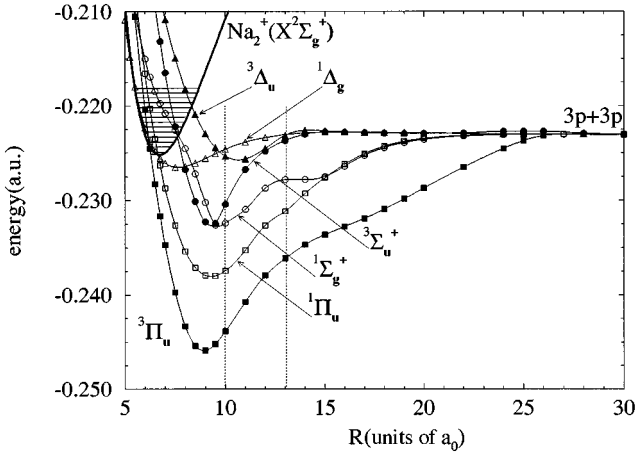

FIG. 1. Potential curves correlated to the dissociation limit $(3p+3p)$ for the symmetries which are likely to contribute to the molecular autoionization reaction. As described in the text, such curves are adiabatic ($\mathcal{A}ni$ states) for $R>13a_0$ and diabatic ($\mathcal{D}pi$ states) for $R<10a_0$. The region between $10a_0$ and $13a_0$ corresponds to the transition between diabatic and adiabatic representation.

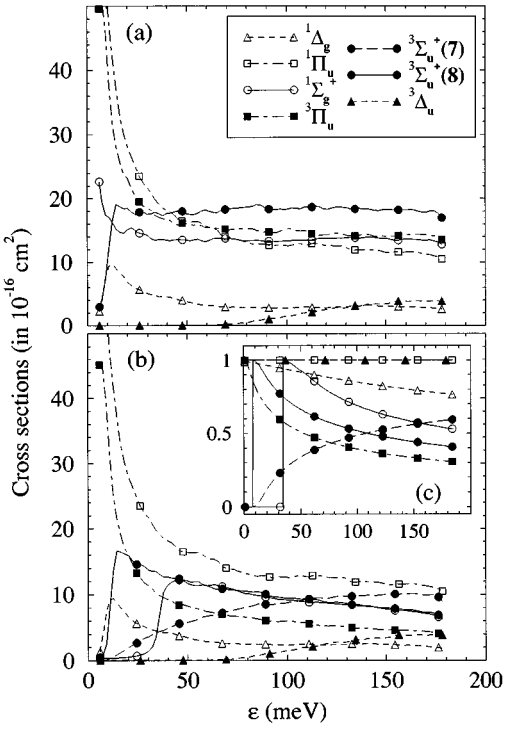

FIG. 2. Molecular autoionization cross sections $\sigma^{\mathrm{MA}}(\mathcal{D}pi;\varepsilon)$, for the symmetries involved in this process, as a function of collision energy, computed in the framework of the MQDT treatment (described in the text). The contribution of the two states $\mathcal{A}7\,{}^3\Sigma_u^+$ and $\mathcal{A}8\,{}^3\Sigma_u^+$ to the $\mathcal{D}2\,{}^3\Sigma_u^+$ channel are denoted by ${}^3\Sigma_u^+(7)$ and ${}^3\Sigma_u^+(8)$, respectively. Calculation (a) assuming population of the short-range doubly excited autoionizing states with unit probability; (b) taking into account long-range population transfers [Eq. (10)]. (In both cases the resonant structure obtained in the calculations [18] has been smoothed by convolution with a Lorentzian energy distribution function of 4-meV width). In (c) the transfer coefficients $w(\mathcal{A}ni\rightarrow\mathcal{D}pi;\varepsilon)$ [Eqs. (10) and (11)] are represented.

excluding the n_i lowest solutions from $\mathcal{P}_i$, which defines the subspace X_i; (iv) building the $\mathcal{Q}_i$ subspace by considering, for each symmetry, doubly excited configurations, for which both electrons occupy excited Na_2^+ orbitals; and (v) diagonalizing the Hamiltonian in $\mathcal{Q}_i'=\mathcal{Q}_i\cup X_i$. When n_i is chosen as the number of dissociation limits $\mathrm{Na}(3s)+\mathrm{Na}(nl)$ of symmetry i below the $\mathrm{Na}(3p)+\mathrm{Na}(3p)$ dissociation limit, diagonalization within the subspace $\mathcal{Q}_i'=\mathcal{Q}_i\cup X_i$ has been shown to provide potential curves that are *diabatic at short range and adiabatic at long range*. Such curves should be relevant for the interpretation of two-color photoassociation spectroscopy experiments. The present theoretical model uses three steps of dynamical calculations.

(i) At short internuclear distances $R<10a_0$, the molecular autoionization process (4) is computed using the MQDT treatment of Ref. [18]. Starting with a short-range diabatic doubly excited state of symmetry i, hereafter labeled $\mathcal{D}pi$ (i.e., the p^{th} level in the doubly excited subspace), we define

TABLE I. Correlation between the adiabatic (long-range) curves $\mathcal{A}n^{2S+1}\Lambda_{g/u}$ [dissociating in $\mathrm{Na}(3p)+\mathrm{Na}(3p)$] and the diabatic (short-range) autoionizing doubly excited curves $\mathcal{D}p^{2S+1}\Lambda_{g/u}$, crossing the ionic Na_2^+ ground-state curve at a distance $\mathcal{D}_{pi}$ and an energy $\mathcal{D}_{pi}$, just above the vibrational level v_c^+ of Na_2^+.

Long-range *adiabatic* representation $\mathcal{A}n^{2S+1}\Lambda_{g/u}$	Short-range *diabatic* representation $\mathcal{D}p^{2S+1}\Lambda_{g/u}$	$R_{\mathcal{D}pi}$ (a.u.)	$\mathcal{E}_{\mathcal{D}pi}-E_{3p+3p}$ (meV)	v_c^+
$\mathcal{A}2\,{}^3\Delta_u$	$\mathcal{D}1\,{}^3\Delta_u$	8.3	+78.2	10
$\mathcal{A}2\,{}^1\Delta_g$	$\mathcal{D}1\,{}^1\Delta_g$	6.4	−56.4	0
$\mathcal{A}4\,{}^3\Pi_u$	$\mathcal{D}1\,{}^3\Pi_u$	6.2	−37.7	1
$\mathcal{A}4\,{}^1\Pi_u$	$\mathcal{D}1\,{}^1\Pi_u$	6.7	−60.5	0
$\mathcal{A}8\,{}^3\Sigma_u^+$	$\mathcal{D}2\,{}^3\Sigma_u^+$	7.6	−10.8	3
$\mathcal{A}8\,{}^1\Sigma_g^+$	$\mathcal{D}2\,{}^1\Sigma_g^+$	7.7	−8.7	3

a total molecular autoionization (MA) cross section, by summing the partial cross sections for reaction (4) over all the vibrational and rotational levels of the final ion, as

$$\sigma^{\mathrm{MA}}(\mathcal{D}pi;\varepsilon)=\sum_{v^+,J^+}\sigma^{\mathrm{MA}}_{\mathrm{part}}[\mathcal{D}pi\rightarrow(v^+,J^+);\varepsilon'].\qquad(9)$$

As in Refs. [18,20], we defined this cross section assuming that the doubly excited state is populated with a unit probability.

At low collision energies ($\varepsilon<70$ meV), it was shown in Ref. [20] that four doubly excited states $\mathcal{D}2\,{}^1\Sigma_g^+$, $\mathcal{D}2\,{}^3\Sigma_u^+$, $\mathcal{D}1\,{}^1\Pi_u$, and $\mathcal{D}1\,{}^3\Pi_u$, and possibly the $\mathcal{D}1\,{}^1\Delta_g$ state, are likely to contribute to the molecular autoionization. In the present work, we have added calculations for the $\mathcal{D}1\,{}^3\Delta_u$ state, which contributes at energies $\varepsilon>70$ meV. The corresponding potential curves defined above in Hund's case *a* coupling scheme (diabatic at short range, adiabatic at long range) are represented in Fig. 1. The coordinates (distance and energy) of the point where they cross the Na_2^+ ground-state potential curve are indicated in Table I: in the following they will be denoted by $R_{\mathcal{D}pi}$ and $\mathcal{E}_{\mathcal{D}pi}$ for the doubly excited state labeled $\mathcal{D}pi$. The variation of the molecular autoioniz-

ation cross sections is represented in Fig. 2(a) as a function of collision energy ε in the 1–180 meV range, and the threshold at 70 meV for the $\mathcal{D}1\,^3\Delta_u$ state is clearly manifested. This energy threshold is close to the difference between $\mathcal{E}_{\mathcal{D}1\,^3\Delta_u}$ and the energy of the $3p+3p$ asymptote (see Table I).

In the present work, the six ionization channels $\mathcal{D}2\,^1\Sigma_g^+$, $\mathcal{D}2\,^3\Sigma_u^+$, $\mathcal{D}1\,^1\Pi_u$, $\mathcal{D}1\,^3\Pi_u$, $\mathcal{D}1\,^1\Delta_g$, and $\mathcal{D}1\,^3\Delta_u$ described above are considered. Each one of them is correlated to *one* long-range adiabatic state $\mathcal{A}ni$ dissociating into $3p+3p$, as indicated in the first two columns of Table I. We are not considering the possibility of ionization via channels corresponding to doubly excited potential curves lying above this set of states.

(ii) In the intermediate-distance range $(10a_0-30a_0)$, long-range pseudocrossings between adiabatic curves are manifested for various symmetries [19,20,27,28] due to interaction between covalent states, dissociating into $\mathrm{Na}(nl)+\mathrm{Na}(n'l')$, and ionic states, dissociating into $\mathrm{Na}^+ + \mathrm{Na}^-$. In the latter case the negative ion is either in the ground state ($^1\Sigma_{g/u}^+$ symmetries) or in an excited autoionizing state ($^3\Pi_{g/u}$ symmetries), stabilized by the Coulomb attraction of the Na^+ ion. A full quantal treatment being not possible at present, we have developed [28,20] a simple multicrossing Landau-Zener model to deal with the flux loss at such pseudocrossings when reaction (3) is taking place. Therefore, although the short-range autoionizing doubly excited state is correlated in our model to *one* long-range adiabatic state, we allow for population transfer between several adiabatic potential curves of the same symmetry through the avoided crossings. We have then defined reduced cross sections as

$$\sigma_{ad}^{\mathrm{MA}}(\mathcal{A}ni;\varepsilon)=w(\mathcal{A}ni\rightarrow\mathcal{D}pi;\varepsilon)\,\sigma^{\mathrm{MA}}(\mathcal{D}pi;\varepsilon) \qquad (10)$$

by using the energy-dependent coefficients w (see Appendix A) to deal with the fractional population which is effectively transmitted into the inner region. This cross section is defined for reactions (3) and (4), and the indexes $\mathcal{A}ni$ on, $\mathcal{D}pi$ in Eqs. (9) and (10) denote, respectively, adiabatic and diabatic molecular states of symmetry i correlated to the $\mathrm{Na}(3p)+\mathrm{Na}(3p)$ limit. For states with $\Lambda\neq 0$, we defined a one-to-one correspondence between $\mathcal{A}ni$ and $\mathcal{D}pi$ states (see Fig. 1 and Table I). In contrast, two adiabatic curves ($\mathcal{A}7i$ and $\mathcal{A}8i$) are correlated to $\mathrm{Na}(3p)+\mathrm{Na}(3p)$ in the case of Σ states ($i=^1\Sigma_g^+$ and $^3\Sigma_u^+$). The model should include not only the population transfers between these symmetries [Eq. (10)], but also a *coherence term* as two different paths ($\mathcal{A}7i$ and $\mathcal{A}8i$) can lead to the same ionization channel ($\mathcal{D}2i$). The cross sections are

$$\sigma_{ad}^{\mathrm{MA}}(\mathcal{A}7i;\varepsilon)=w(\mathcal{A}7i\rightarrow\mathcal{D}2i;\varepsilon)\,\sigma^{\mathrm{MA}}(\mathcal{D}2i;\varepsilon),$$

$$\sigma_{ad}^{\mathrm{MA}}(\mathcal{A}8i;\varepsilon)=w(\mathcal{A}8i\rightarrow\mathcal{D}2i;\varepsilon)\,\sigma^{\mathrm{MA}}(\mathcal{D}2i;\varepsilon), \qquad (11)$$

and the coherence term

$$\begin{aligned} u_{ad}^{\mathrm{MA}}(\mathcal{A}[7,8]i;\varepsilon)&=[w(\mathcal{A}7i\rightarrow\mathcal{D}2i;\varepsilon)]^{1/2}\\ &\quad\times[w(\mathcal{A}8i\rightarrow\mathcal{D}2i;\varepsilon)]^{1/2}\sigma^{\mathrm{MA}}(\mathcal{D}2i;\varepsilon)\\ &=f_{ad}^{\mathrm{MA}}(\mathcal{A}7i;\varepsilon)\,f_{ad}^{\mathrm{MA}}(\mathcal{A}8i;\varepsilon). \end{aligned} \qquad (12)$$

In Eq. (12), we assumed that we can define effective (real) transition amplitudes, averaged on all impact parameter values involved in the process, as

$$f_{ad}^{\mathrm{MA}}(\mathcal{A}ni;\varepsilon)=[w(\mathcal{A}ni\rightarrow\mathcal{D}2i;\varepsilon)]^{1/2}[\sigma^{\mathrm{MA}}(\mathcal{D}2i;\varepsilon)]^{1/2}. \qquad (13)$$

The cross sections $\sigma_{ad}^{\mathrm{MA}}(\mathcal{A}ni;\varepsilon)$ are plotted in Fig. 2(b), and the transfer coefficients $w(\mathcal{A}ni\rightarrow\mathcal{D}pi;\varepsilon)$ in Fig. 2(c). As

TABLE II. Projection of the initial states $(j_A=\frac{3}{2},m_A;j_B=\frac{3}{2},m_B)$ of the separated atoms on the molecular asymptotic states of symmetry $^{2S+1}\Lambda_{g/u}$, assuming a sudden approximation. The sign in brackets indicates that the projection involves the positive (+), or negative (−), or both (±) components of the states with $\Lambda\neq 0$.

(m_A,m_B)	$^3\Delta_u$	$^1\Delta_g$	$^3\Pi_u$	$^1\Pi_u$	$^3\Pi_g$	$^1\Pi_g$	$^1\Sigma_u^-(\pi\pi)$	$^3\Sigma_u^+(\pi\pi)$	$^3\Sigma_u^+(\sigma\sigma)$	$^3\Sigma_g^-(\pi\pi)$	$^1\Sigma_g^+(\pi\pi)$	$^1\Sigma_g^+(\sigma\sigma)$
$(\frac{3}{2},\frac{3}{2})^{[+]}$	1	0	0	0	0	0	0	0	0	0	0	0
$(\frac{3}{2},\frac{1}{2})^{[+]}$	$1/\sqrt{6}$	$1/\sqrt{6}$	$1/\sqrt{3}$	0	$1/\sqrt{3}$	0	0	0	0	0	0	0
$(\frac{3}{2},-\frac{1}{2})^{[+]}$	0	0	$1/\sqrt{6}$	$1/\sqrt{6}$	$1/\sqrt{6}$	$1/\sqrt{6}$	0	$1/\sqrt{6}$	0	$1/\sqrt{6}$	0	0
$(\frac{3}{2},-\frac{3}{2})$	0	0	0	0	0	0	1/2	1/2	0	1/2	1/2	0
$(\frac{1}{2},\frac{3}{2})^{[+]}$	$1/\sqrt{6}$	$-1/\sqrt{6}$	$1/\sqrt{3}$	0	$-1/\sqrt{3}$	0	0	0	0	0	0	0
$(\frac{1}{2},\frac{1}{2})^{[+]}$	1/3	0	$\sqrt{2}/3$	$-\sqrt{2}/3$	0	0	0	0	2/3	0	0	0
$(\frac{1}{2},-\frac{1}{2})^{[\pm]}$	0	0	1/3	0	1/3	0	−1/6	1/6	$\sqrt{2}/3$	1/6	−1/6	$\sqrt{2}/3$
$(\frac{1}{2},-\frac{3}{2})^{[-]}$	0	0	$1/\sqrt{6}$	$1/\sqrt{6}$	$1/\sqrt{6}$	$1/\sqrt{6}$	0	$1/\sqrt{6}$	0	$1/\sqrt{6}$	0	0
$(-\frac{1}{2},\frac{3}{2})^{[+]}$	0	0	$1/\sqrt{6}$	$1/\sqrt{6}$	$-1/\sqrt{6}$	$-1/\sqrt{6}$	0	$1/\sqrt{6}$	0	$-1/\sqrt{6}$	0	0
$(-\frac{1}{2},\frac{1}{2})^{[\pm]}$	0	0	1/3	0	−1/3	0	−1/6	1/6	$\sqrt{2}/3$	−1/6	1/6	$-\sqrt{2}/3$
$(-\frac{1}{2},-\frac{1}{2})^{[-]}$	1/3	0	$\sqrt{2}/3$	$-\sqrt{2}/3$	0	0	0	0	2/3	0	0	0
$(-\frac{1}{2},-\frac{3}{2})^{[-]}$	$1/\sqrt{6}$	$1/\sqrt{6}$	$1/\sqrt{3}$	0	$1/\sqrt{3}$	0	0	0	0	0	0	0
$(-\frac{3}{2},\frac{3}{2})$	0	0	0	0	0	0	1/2	1/2	0	−1/2	−1/2	0
$(-\frac{3}{2},\frac{1}{2})^{[-]}$	0	0	$1/\sqrt{6}$	$1/\sqrt{6}$	$-1/\sqrt{6}$	$-1/\sqrt{6}$	0	$1/\sqrt{6}$	0	$-1/\sqrt{6}$	0	0
$(-\frac{3}{2},-\frac{1}{2})^{[-]}$	$1/\sqrt{6}$	$-1/\sqrt{6}$	$1/\sqrt{3}$	0	$-1/\sqrt{3}$	0	0	0	0	0	0	0
$(-\frac{3}{2},-\frac{3}{2})^{[-]}$	1	0	0	0	0	0	0	0	0	0	0	0

discussed in Ref. [20], the population transfer reduces mainly the population of the $\mathcal{D}1\,^3\Pi_u$ short-range state, due to an ionic-covalent pseudocrossing at $R=26a_0$, which, moreover, strongly mixes the contribution of the $\mathcal{A}7$ and $\mathcal{A}8$ $3\Sigma_u^+$ states. The introduction of the w coefficients in the model is made necessary due to the large values of the energy pooling cross sections, which are a manifestation of an important population transfer in the vicinity of some pseudocrossings.

(iii) In the long-distance range ($R>30a_0$), the change from an atomic to a molecular basis and the spin-uncoupling effect should be taken into account. This change depends markedly upon the collision energy considered, and the evolution from one Hund's case coupling scheme to another one is a particularly important point [29], which might also be crucial even at smaller distances [20]. In the present work, we considered a simple model with sudden approximation for spin uncoupling, and infinite locking radius. The locking phenomenon has been discussed in several papers [30–34] in the case of a P-state atom interacting with a ^1S atom: only two molecular symmetries are then considered, and a ''locking radius'' R_L can easily be estimated as an integral involving the two corresponding potential curves. Generalization of such a model to the more complex situation of two interacting P-state atoms, where many molecular symmetries are involved, still has to be developed. In a recent discussion by Yurova [35] on polarization effects in energy pooling collisions, the locking radius was estimated for various pairs of states, considering each time an isolated two-state system. The large values obtained ($R_L>50$ a.u.), as compared with the relatively small range of impact parameters involved in the associative ionization reaction ($b<$ a.u.) suggest that the ''locking angle'' would be very small ($<8°$): therefore, the hypothesis of an infinite locking radius could be reasonable. However, a correct evaluation of the population transfer at large internuclear distances would require solution of quantal coupled equations in connection with the MQDT treatment at short distances, which is beyond the possibilities of the existing theoretical tools.

We assume that the various Hund's case a molecular states correlated to the $\mathrm{Na}(3p)+\mathrm{Na}(3p)$ limit share statistically the population of the different combinations of the fine-structure components (j_A,j_B) of the atomic $3p$ level. Indeed, we do not consider the possibility of adiabatic correlation through Hund's case c curves to a specific (j_A,j_B) asymptote, as for the $\mathcal{A}4\,^3\Pi_u$ state, which should be preferentially populated from the $(j_A=\frac{1}{2},\ j_B=\frac{1}{2})$ or the $(j_A=\frac{1}{2},\ j_B=\frac{3}{2})$ asymptotic levels [36]. This particular hypothesis will be discussed in Sec. IV B. The cross section for the associative ionization reaction corresponding to the three steps (2)–(4) is then compactly written as

$$\sigma_{\mathrm{tot}}^{\mathrm{AI}}(j_Am_A,j_Bm_B)=\sum_i\sum_p\sum_{n,n'}\zeta(j_Am_A,j_Bm_B;\mathcal{A}ni)\times\zeta(j_Am_A,j_Bm_B;\mathcal{A}n'i)\times[w(\mathcal{A}ni\rightarrow\mathcal{D}pi;\varepsilon)w(\mathcal{A}n'i\rightarrow\mathcal{D}pi;\varepsilon)]^{1/2}\times\sigma^{MA}(\mathcal{D}pi;\varepsilon). \tag{14}$$

The so-called coherence terms [14] are also defined:

$$u_{\mathrm{tot}}^{\mathrm{AI}}(j_Am_A,j_Bm_B;j_A'm_A',j_B'm_B')=\sum_i\sum_p\sum_{n,n'}\zeta(j_Am_A,j_Bm_B;\mathcal{A}ni)\zeta(j_A'm_A',j_B'm_B';\mathcal{A}n'i)\times[w(\mathcal{A}ni\rightarrow\mathcal{D}pi;\varepsilon)w(\mathcal{A}n'i\rightarrow\mathcal{D}pi;\varepsilon)]^{1/2}\times\sigma^{MA}(\mathcal{D}pi;\varepsilon), \tag{15}$$

where the coefficients ζ's are the expansion coefficients of a particular initial atomic state (j_Am_A,j_Bm_B) projected onto the various adiabatic states $\mathcal{A}ni$ in the spin-uncoupling scheme. As discussed in (ii) above, the indexes n and n' in Eqs. (14) and (15) are equal, except for Σ symmetries. In our model the efficient channels of different symmetries $^{2S+1}\Lambda_{g/u}$ participate independently in the molecular ionization. It follows that the coherence of two different initial states (j_Am_A,j_Bm_B) and $(j_A'm_A',j_B'm_B')$ also leads to a cross-section term instead of a product of complex ionization amplitudes. In Table II we give the projection coefficients, hereafter denoted by $\xi_{\mathrm{asymp}}(j_A=j_B=\frac{3}{2},m_A,m_B;i)$, of all the combinations of Zeeman substates (m_A,m_B) onto the asymptotic molecular states constructed from products of atomic orbitals in L picture. For the $^3\Delta_u$, $^1\Delta_g$, $^3\Pi_u$, $^1\Pi_u$ symmetries, which are connected to only one atomic configuration, these coefficients are then identified with the numbers $\zeta(j_Am_A,j_Bm_B,\mathcal{A}ni)$ (with $j_A=j_B=\frac{3}{2}$), which appear in Eqs. (14) and (15) and represent the projections of the various initial states (m_A,m_B) on the adiabatic states $\mathcal{A}ni$. For the $^3\Sigma_u^+$ and $^1\Sigma_g^+$ symmetries, the sudden approximation provides two asymptotic states represented by the product of atomic orbitals ''$3p\sigma,3p\sigma$'' or ''$3p\pi,3p\pi$'' (hereafter denoted by ''$\sigma\sigma$'' or ''$\pi\pi$''). The $\mathcal{A}7,8\,^3\Sigma_u^+$ and $\mathcal{A}7,8\,^1\Sigma_g^+$ adiabatic states resulting from the *ab initio* calculations are combinations of the $\sigma\sigma$ and $\pi\pi$ asymptotic states, expressed via a rotation matrix:

$$\begin{pmatrix}^3\Sigma_u^+(\pi\pi)\\ ^3\Sigma_u^+(\sigma\sigma)\end{pmatrix}=\begin{pmatrix}\cos\alpha_T & \sin\alpha_T\\ \sin\alpha_T & -\cos\alpha_T\end{pmatrix}\begin{pmatrix}7\,^3\Sigma_u^+\\ 8\,^3\Sigma_u^+\end{pmatrix}. \tag{16}$$

The same relation holds for $^1\Sigma_g^+$, with angle α_S. Therefore, for the $^3\Sigma_u^+$ and $^1\Sigma_g^+$ symmetries, the numbers $\zeta(j_Am_A,j_Bm_B;\mathcal{A}ni)$ are expressed in terms of the $\xi_{\mathrm{asymp}}(j_A=j_B=\frac{3}{2},m_A,m_B;i)$'s via the rotation matrix in Eq. (16). We have deduced the values for the mixing angles α_T and α_S from the *ab initio* potential calculations of [19]:

$$\cos\alpha_T=0.8,\quad \sin\alpha_T=0.6,\quad \alpha_T=37°. \tag{17}$$

The value of α_S is also close to 37°.

However, due to the dynamical coupling between the two adiabatic states $\mathcal{A}7i$ and $\mathcal{A}8i$, the mixing angles α_T and α_S may also be considered, in a crude model, as free parameters accounting for this coupling. Then every step of the present model may be described in a very general way as successive unitary transformations from an initial atomic state (m_A,m_B) to the final doubly excited states $(\mathcal{D}1i)$ and $(\mathcal{D}2i)$ (with $i=^1\Sigma_g^+,\ ^3\Sigma_u^+$):

$$\begin{pmatrix} m_A m_B \\ m'_A m'_B \end{pmatrix} = \hat{\xi}\begin{pmatrix} \pi\pi \\ \sigma\sigma \end{pmatrix} = \hat{\xi}\cdot\hat{\alpha}\begin{pmatrix} \mathcal{A}7i \\ \mathcal{A}8i \end{pmatrix} = \hat{\xi}\cdot\hat{\alpha}\cdot\hat{\beta}\begin{pmatrix} \mathcal{D}1i \\ \mathcal{D}2i \end{pmatrix}$$
$$= \begin{pmatrix} \xi_{\pi\pi} & \xi_{\sigma\sigma} \\ \xi'_{\pi\pi} & \xi'_{\sigma\sigma} \end{pmatrix}\begin{pmatrix} \cos\alpha & \sin\alpha \\ \sin\alpha & -\cos\alpha \end{pmatrix}$$
$$\times\begin{pmatrix} \cos\beta(\varepsilon) & \sin\beta(\varepsilon) \\ -\sin\beta(\varepsilon) & \cos\beta(\varepsilon) \end{pmatrix}\begin{pmatrix} \mathcal{D}1i \\ \mathcal{D}2i \end{pmatrix}. \quad (18)$$

The matrices $\hat{\xi}$ and $\hat{\alpha}$ correspond to simple geometric transformations, with $\alpha=\alpha_T$, α_S and $\xi=\xi^T$, ξ^S for the $^3\Sigma_u^+$ and $^1\Sigma_g^+$ symmetries, respectively. It is easy to see that their product yields the $\zeta(j_A m_A, j_B m_B; \mathcal{A}ni)$ coefficients used in Eqs. (14) and (15). The matrix $\hat{\beta}$ accounts for the energy-dependent population sharing between the two adiabatic states [with $\beta(\varepsilon)=\beta_T(\varepsilon)$, $\beta_S(\varepsilon)$], leading to the doubly excited states. In our model, only the $\mathcal{D}2i$ channel leads to autoionization. We can formally write, from Eqs. (10)–(15),

$$\cos\beta(\varepsilon)=[w(\mathcal{A}7i\rightarrow\mathcal{D}1i;\varepsilon)]^{1/2}=[w(\mathcal{A}8i\rightarrow\mathcal{D}2i;\varepsilon)]^{1/2},$$
$$\sin\beta(\varepsilon)=[w(\mathcal{A}7i\rightarrow\mathcal{D}2i;\varepsilon)]^{1/2}=[w(\mathcal{A}8i\rightarrow\mathcal{D}1i;\varepsilon)]^{1/2}, \quad (19)$$

and we verify in Fig. 2(c) that the following identity is indeed fulfilled:

$$w(\mathcal{A}7i\rightarrow\mathcal{D}2i;\varepsilon)+w(\mathcal{A}8i\rightarrow\mathcal{D}2i;\varepsilon)=1. \quad (20)$$

Owing to the fact that the symmetry $^1\Sigma_g^+$ makes a weaker contribution to the process (its statistical weight is one-third of that of $^3\Sigma_u^+$, for instance), we simplified the model by introducing a variable angle α_T and setting $\alpha_S=0$. This means we correlate the $\mathcal{A}7\ ^1\Sigma_g^+$ state to its asymptotic component $\pi\pi$, and the $\mathcal{A}8\ ^1\Sigma_g^+$ state to the $\sigma\sigma$ one. In Sec. IV, we will present results corresponding to several choices for the mixing angle α_T, while the functions $\beta(\varepsilon)=\beta_T(\varepsilon)$, $\beta_S(\varepsilon)$ are determined using a Landau-Zener picture, as explained in (ii) above, and averaging over impact parameters. From Eqs. (18) and (19), this procedure can be generalized by keeping α_T at a fixed value (yielded, for instance, by the *ab initio* calculations), and by varying the functions $\beta(\epsilon)$ to reproduce experimental results. The coupling between the two adiabatic states over all distances may then be included in the model, through the energy-dependent parameters $\beta(\varepsilon)=\beta_T(\varepsilon)$, $\beta_S(\varepsilon)$.

In order to provide cross sections directly comparable to experimental data, the populations of the initial magnetic sublevels $(j_A m_A)$ and $(j_B m_B)$ (projected onto the body-fixed frame) have to be determined, according to the excitation scheme, i.e., the polarization of the laser light exciting each atom and the geometry of experiment. We shall represent the excitation scheme by the combined symbol $[\tilde{\alpha}_A,\tilde{\alpha}_B]$, so that the populations are entirely characterized by the atomic density matrices $\varrho_A(j_A,\tilde{\alpha}_A)$ and $\varrho_B(j_B,\tilde{\alpha}_B)$ of the collision partners. Summing over all possible initial states (m_A,m_B), we define the total AI cross section for the excitation scheme $[\tilde{\alpha}_A,\tilde{\alpha}_B]$ and for the relative collision energy ε as

$$\sigma^{\mathrm{AI}}_{\mathrm{TOT}}(j_A j_B,\tilde{\alpha}_A\tilde{\alpha}_B;\varepsilon)=\sum_{m_A m_B}\sum_{m'_A m'_B}\sum_i\sum_p\sum_{n,n'}\zeta(j_A m_A,j_B m_B;\mathcal{A}ni)\zeta(j'_A m'_A,j'_B m'_B;\mathcal{A}n'i)$$
$$\times[w(\mathcal{A}ni\rightarrow\mathcal{D}pi;\varepsilon)w(\mathcal{A}n'i\rightarrow\mathcal{D}pi;\varepsilon)]^{1/2}\eta(j_A m_A,j_B m_B;j'_A m'_A,j'_B m'_B)$$
$$\times\langle m_A|\varrho_A(j_A,\tilde{\alpha}_A)|m'_A\rangle\langle m_B|\varrho_B(j_B,\tilde{\alpha}_B)|m'_B\rangle\sigma^{\mathrm{MA}}(\mathcal{D}pi;\varepsilon). \quad (21)$$

This equation includes not only the cross sections (11) and (14), but also the coherence terms of Eqs. (12) and (15), which have often been neglected in previous theoretical models. The function $\eta(j_A m_A,j_B m_B;j'_A m'_A j'_B m'_B)$ depends upon the geometry of the experimental setup: for a single beam, colinear beam (both corresponding to cylindrical symmetry of the setup) and orthogonal beam (with the same quantization axis for both beams) experiments, contributing terms to Eq. (21) satisfy the conservation relation [14]

$$\eta(j_A m_A,j_B m_B;j'_A m'_A,j'_B m'_B)=\delta(m_A+m_B,m'_A+m'_B), \quad (22)$$

while, for an isotropic cell experiment,

$$\eta(j_A m_A,j_B m_B;j'_A m'_A,j'_B m'_B)=1. \quad (23)$$

It is worthwhile to write Eq. (21) as a weighted sum of the molecular autoionization cross sections for the various symmetries pi previously defined by Eq. (9):

$$\sigma^{\mathrm{AI}}_{\mathrm{TOT}}(j_A j_B,\tilde{\alpha}_A\tilde{\alpha}_B;\varepsilon)$$
$$=\sum_{p,i}\Xi_{j_A j_B}(\mathcal{D}pi;\tilde{\alpha}_A\tilde{\alpha}_B;\varepsilon)\sigma^{\mathrm{MA}}(\mathcal{D}pi;\varepsilon). \quad (24)$$

In Eq. (24), we introduced the molecular weights as

TABLE III. Various combinations of initial diatomic states $[(m_A,m_B),\ (m'_A,m'_B)]$ (with $j_A=j_B=\frac{3}{2}$) that are likely to contribute *coherently* to the molecular autoionization signal via a channel of symmetry $i={}^{2S+1}\Lambda_{g/u}$. We assume that the condition $m_A+m_B=m'_A+m'_B$ is verified (see text).

${}^{2S+1}\Lambda_{g/u}$	$[(m_A,m_B);(m'_A,m'_B)]$
${}^3\Delta_u\ {}^1\Delta_g$	$[(\frac{3}{2},\frac{1}{2});(\frac{1}{2},\frac{3}{2})]\ [(-\frac{1}{2},-\frac{3}{2});(-\frac{3}{2},-\frac{1}{2})]$
${}^3\Pi_u$	$[(\frac{3}{2},\frac{1}{2});(\frac{1}{2},\frac{3}{2})]\ [(-\frac{1}{2},-\frac{3}{2});(-\frac{3}{2},-\frac{1}{2})]$ $[(\frac{3}{2},-\frac{1}{2});(\frac{1}{2},\frac{1}{2})]\ [(\frac{3}{2},-\frac{1}{2});(-\frac{1}{2},\frac{3}{2})]\ [(\frac{1}{2},\frac{1}{2});(-\frac{1}{2},\frac{3}{2})]$ $[(\frac{1}{2},-\frac{3}{2});(-\frac{1}{2},-\frac{1}{2})]\ [(\frac{1}{2},-\frac{3}{2});(-\frac{3}{2},\frac{1}{2})]\ [(-\frac{1}{2},-\frac{1}{2});(-\frac{3}{2},\frac{1}{2})]$
${}^1\Pi_u$	$[(\frac{3}{2},-\frac{1}{2});(\frac{1}{2},\frac{1}{2})]\ [(\frac{3}{2},-\frac{1}{2});(-\frac{1}{2},\frac{3}{2})]\ [(\frac{1}{2},\frac{1}{2});(-\frac{1}{2},\frac{3}{2})]$ $[(\frac{1}{2},-\frac{3}{2});(-\frac{1}{2},-\frac{1}{2})]\ [(\frac{1}{2},-\frac{3}{2});(-\frac{3}{2},\frac{1}{2})]\ [(-\frac{1}{2},-\frac{1}{2});(-\frac{3}{2},\frac{1}{2})]$
$7\ {}^3\Sigma_u^+, 8\ {}^3\Sigma_u^+$	$[(\frac{3}{2},-\frac{1}{2});(\frac{1}{2},\frac{1}{2})]\ [(\frac{3}{2},-\frac{1}{2});(-\frac{1}{2},\frac{3}{2})]\ [(\frac{1}{2},\frac{1}{2});(-\frac{1}{2},\frac{3}{2})]$ $[(\frac{1}{2}-\frac{3}{2});(-\frac{1}{2},-\frac{1}{2})]\ [(\frac{1}{2},-\frac{3}{2});(-\frac{3}{2},\frac{1}{2})]\ [(-\frac{1}{2},-\frac{1}{2});(-\frac{3}{2},\frac{1}{2})]$ $[(\frac{1}{2},-\frac{1}{2});(\frac{3}{2},-\frac{3}{2})]$
${}^1\Sigma_g^+$	$[(\frac{1}{2};-\frac{1}{2});(\frac{3}{2},-\frac{3}{2})]$

$$\Xi_{j_Aj_B}(\mathcal{D}pi;\tilde{\alpha}_A\tilde{\alpha}_B;\varepsilon)=\sum_{m_Am_B}\sum_{m'_Am'_B}\sum_{n,n'}\zeta(j_Am_A,j_Bm_B;\mathcal{A}ni)\zeta(j'_Am'_A,j'_Bm'_B;\mathcal{A}n'i)[w(\mathcal{A}ni\rightarrow\mathcal{D}pi;\varepsilon)w(\mathcal{A}n'i\rightarrow\mathcal{D}pi;\varepsilon)]^{1/2}\eta(j_Am_A,j_Bm_B;j'_Am'_A,j'_Bm'_B)\langle m_A|\varrho_A(j_A,\tilde{\alpha}_A)|m'_A\rangle\langle m_B|\varrho_B(j_B,\tilde{\alpha}_B)|m'_B\rangle. \quad (25)$$

In the model developed in the present paper, the autoionization cross sections are defined assuming a unit population of a short-range doubly excited state, whereas the molecular weights contain all the information concerning the long-range dynamics, i.e., the population transfer from the initial preparation of the two atoms to the short-range autoionizing states $\mathcal{D}pi$. Indeed, Eq. (25) includes *all* the contributions, in particular the *coherences*, of the various possible initial states (j_Am_A) and (j_Bm_B), to the population of the adiabatic states $\mathcal{A}ni$. As an example, in Table III we display the various pairs $[(m_A,m_B);(m'_A,m'_B)]$ of initial diatomic states (for $j_A=j_B=\frac{3}{2}$) leading to coherent contributions to the cross section for each molecular symmetry. Furthermore, through the transmission factors w (see Appendix A), the molecular weights Ξ take into account the long-range radial coupling between the adiabatic states $\mathcal{A}ni$ of a same symmetry i, and then describe how the molecular population is transmitted to the inner region. Finally, the dependence upon the excitation scheme (polarization of the exciting laser and geometry of excitation) of the initial atomic states is described by the density matrices $\varrho_A(j_A,\tilde{\alpha}_A)$ and $\varrho_B(j_B,\tilde{\alpha}_B)$.

In order to compare with experiment, the cross section in Eqs. (21) or (24) has to be convoluted with the distribution $D(v_c)$ of the relative velocities $v_c=\sqrt{2\mu\varepsilon}$ of the two colliding atoms, where μ is the reduced mass:

$$\overline{\sigma^{\mathrm{AI}}_{\mathrm{TOT}}}(j_Aj_B,\tilde{\alpha}_A\tilde{\alpha}_B;\overline{v_c})=\int\sigma^{\mathrm{AI}}_{\mathrm{TOT}}(j_Aj_B,\tilde{\alpha}_A\tilde{\alpha}_B;v_c)D(v_c)dv_c, \quad (26)$$

leading to the rate constant:

$$R^{\mathrm{AI}}(j_Aj_B,\tilde{\alpha}_A\tilde{\alpha}_B;\overline{v_c})=\int v_c\sigma^{\mathrm{AI}}_{\mathrm{TOT}}(j_Aj_B,\tilde{\alpha}_A\tilde{\alpha}_B;v_c)D(v_c)dv_c. \quad (27)$$

The velocity distributions, $D(v_c)$ are defined in the experimental papers discussed in Sec. III, and their expressions are reported in Appendix B. Further details concerning the averaging procedure can be found in Ref. [5].

III. DESCRIPTION OF THE VARIOUS EXPERIMENTAL SCHEMES

The total cross section has been measured by Huennekens and Gallagher [2] in a cell experiment exciting both the D_1 and D_2 lines with an unpolarized laser. For this experiment, the velocity distribution is a Maxwellian distribution [given by Eq. (B1) in Appendix B]. The atomic populations are equally distributed over the sublevels $m_{l,A}$ and $m_{l,B}$ of the $3p\ {}^2P$ state, due to rapid collisional mixing in an isotropic medium at relatively high temperatures ($\approx$650 K) [2]. Therefore, the atomic density matrices ϱ_{cell}, required to calculate this cross section through Eq. (21), may be considered in the L picture and will be diagonal, with equal elements given by a suitable normalization condition. Accordingly, all the possible combinations for $j_A=\frac{1}{2}$, $j_B=\frac{3}{2}$ have been included. The experimental data are compared to our results in Fig. 3.

Crossed-beam experiments were performed by the Utrecht group [3,4] with two counterpropagating thermal sodium beams, the collision velocity range covered by this ex-

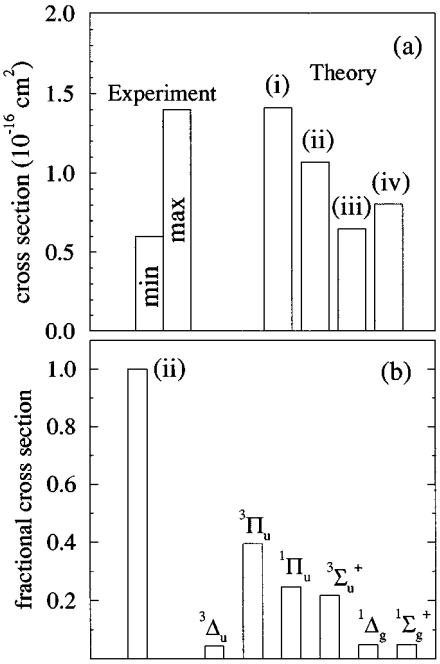

FIG. 3. Computed total cross section $\overline{\sigma}^{\mathrm{Al}}_{\mathrm{TOT}}$ (with $\alpha_T=37°$) compared to experiment. (i) All symmetries included, and with the unit transfer coefficient for $^3\Pi_u$: $w(\mathcal{A}4\,^3\Pi_u\rightarrow\mathcal{D}1\,^3\Pi_u;\varepsilon)=1$. (ii) All symmetries included, and with $w(\mathcal{A}4\,^3\Pi_u\rightarrow\mathcal{D}1\,^3\Pi_u;\varepsilon)$ of Fig. 2(c). (iii) All symmetries except $^3\Pi_u$ included. (iv) All symmetries except $^1\Pi_u$ included. (a) The minimum and maximum experimental values of Ref. [2] are reported. (b) Relative contributions to the computed cross section from the various autoionizing channels.

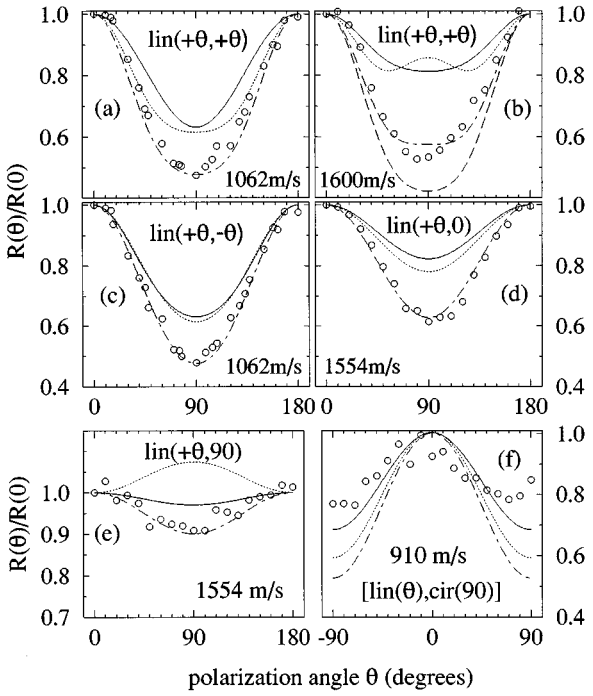

FIG. 4. Associative ionization rate constants $R^{\mathrm{Al}}(3/2,3/2,\widetilde{\alpha}_A,\widetilde{\alpha}_B,\overline{v_c})$ [abbreviated as $R(\theta)$, and normalized at $\theta=0°$] for counterpropagating beams experiments, as a function of the polarization angle θ, for different excitations schemes and different average collision velocities $\overline{v_c}$. Solid line: all molecular symmetries are considered. Dotted line: all symmetries except $^3\Pi_u$ are considered. Dot-dashed line idem, but with an adjusted ($\alpha_T=63°$) mixing between the asymptotic $\sigma\sigma$ and $\pi\pi$ components of the $^3\Sigma_u^+$ states. Long-dashed line in (b): idem, but also excluding $^3\Delta_u$. Circles: experimental results of the Utrecht group [3,4].

perimental setup being (910–2318 m/s). A laser beam tuned on the transition Na $3s\ ^2S_{1/2}(F=2)\rightarrow$Na $3p\ ^2P_{3/2}(F=3)$ and reflected by a perpendicular mirror was intersecting the beams direction at an angle $\alpha\approx 87°$, so that the atoms in the two beams may be excited according to the same geometry, one group (A) by the incident laser beam, the other one (B) by the reflected one. Measurements were performed in various excitation schemes $[\widetilde{\alpha}_A,\widetilde{\alpha}_B]$ corresponding to different polarizations (linear or circular) of the exciting laser beams and different excitation geometries. In each of these schemes, one varies the angle θ between the polarization vector of the laser and the direction of the relative velocity. We report the results in Figs. 4(a)–4(f). In some experiments [3,4] both collision partners were excited with linearly polarized light with the same variable polarization angle θ, the corresponding $[\widetilde{\alpha}_A,\widetilde{\alpha}_B]$ scheme is denoted by lin$(+\theta,+\theta)$ [see Figs. 4(a) and 4(b)]. In another experiment [4], the polarization angles for the two beams were opposite: this is the lin$(+\theta,-\theta)$ scheme, for which the results are represented in Fig. 4(c). For the results reported in Figs. 4(d) and 4(e), the polarization angle varied for one beam, and fixed respectively to 0° and 90° for the other [4]. The corresponding $[\widetilde{\alpha}_A,\widetilde{\alpha}_B]$ schemes are written as lin$(+\theta,0)$ and lin$(+\theta,90)$, respectively. Finally, a mixed polarization excitation scheme, $\lfloor$lin(θ),cir$^+(90)\rfloor$, was also realized [4], in which the direct laser beam exciting atoms A was linearly polarized, with variable θ, while the reflected one exciting atoms B was circularly polarized [see Fig. 4(f)]. The most striking feature of the results, in the case of linear polarization, is a symmetrical variation of the ion signal, when the polarization angle is varied from 0° to 180°, with a minimum at $\theta=90°$. The ion signal is proportional to the rate $R^{\mathrm{Al}}(j_A=\frac{3}{2},j_B=\frac{3}{2};\widetilde{\alpha}_A\widetilde{\alpha}_B;\overline{v_c})$ [see Eq. (27)], hereafter abbreviated as $R(\theta)$. We will consider the normalized signal $R(\theta)/R(0°)$ and define the *angular contrast* C as

$$C=[R(0°)-R(90°)]/R(0°). \tag{28}$$

This contrast is more pronounced at low collision velocities, and decreases when the velocity is increased until a plateau appears at $\overline{v_c}=1960$ m/s in the lin$(+\theta,+\theta)$ scheme. For the ''mixed'' excitation scheme, the ion signal is measured between $-90°$ and $+90°$ and is almost symmetrical with respect to 0°, where it presents a maximum. The velocity distribution for these experiments are discussed in the Appendix B.

A single-beam experiment was performed by Meijer [5] in the 250–500 m/s collision velocity range with only one excitation scheme $[\widetilde{\alpha}_A,\widetilde{\alpha}_B]=lin(+\theta,+\theta)$, where both collision partners are excited by linearly polarized light, with the same variable polarization angle θ. The data are reported in Fig. 6. As in the case of counterpropagating beams, the angular variation of the ion signal from 0° to 180° is symmetrical with respect to 90°, where it presents a minimum. But the angular contrast now increases with increasing collision velocities, and tends to a saturation around 480 m/s.

The experiments of the Maryland group used a different geometry, and considered either two perpendicular thermal beams [6–8] or a single beam [9,10]. The high-resolution velocity selection was achieved through Doppler effect by selecting a particular class of velocity within each beam, or two different velocity groups within the same beam. As the width of the velocity distribution did not exceed 30 m/s, we have checked that the energy dependence of the cross sections (see Fig. 2) is too slow to be affected by convolution with the experimental distribution, so that, for this series of experiments, we can directly compare our calculations for various velocities to the experimental signal (see Fig. 9). The different experiments with their excitation schemes and energy domain are summarized in Table IV, where the correspondence between the excitation schemes used in Maryland and in Utrecht is established.

IV. COMPARISON BETWEEN THEORETICAL AND EXPERIMENTAL RESULTS

Our velocity-dependent molecular autoionization cross sections having been computed in an earlier work [20], we shall compare our results with the experimental ion signal up to a collision velocity of 1750 m/s. Due to the large number of possible autoionization channels, it is worthwhile to use this comparison in order to discuss how a set of experimental results can be used to identify the channels that effectively contribute to the ion formation.

We shall discuss both absolute data, for which the autoionization efficiency of a given channel is the important point, and relative measurements, where the polarization dependence of the ion signal can be considered as a signature of a given molecular symmetry. Within the model developed in the present paper and for the experiments discussed here, the shape of the curve giving the ion signal as a function of the polarization angle may be analyzed by considering both the autoionization efficiency and the θ variation of the weights $\Xi_{j_A j_B}(\mathcal{D}pi;\widetilde{\alpha}_A\widetilde{\alpha}_B;\varepsilon)$ for the different channels contributing to the Al process at the energy ε. The signature of a given doubly excited autoionizing state $\mathcal{D}pi$ will then be manifested by the sign and magnitude of the contrast defined in Eq. (28).

Many interpretations in the past rely upon a unique $^3\Sigma_u^+(\sigma\sigma)$ autoionizing channel. We shall therefore discuss the experimental results by varying in our model the mixing angle α_T for the two long-range components in the $^3\Sigma_u^+$ ionization channel, and by discussing the influence of the other symmetries, in particular the $^3\Pi_u$ channel, which was not considered in previous interpretations of experimental data, and which could be the dominant one, according to the previous discussion concerning autoionization efficiency (see Fig. 2) and to its statistical weight.

A. Total cross section

As mentioned above, the total cross section corresponding to the cell experiment of Ref. [2] may be computed according to Eq. (21) with diagonal atomic density matrices in the L picture for the excited state $3p$. After averaging over the Maxwell velocity distribution [Eq. (B5), Appendix B], our estimation for this cross section for associative ionization of sodium atoms at 650 K is

$$\overline{\sigma_{\mathrm{TOT}}^{\mathrm{AI}}}(\mathrm{cell}, T=650\ \mathrm{K}) = 1.07\times 10^{-16}\ \mathrm{cm}^2 \quad (\pm 7\%).$$

This result has to be compared with the experimental value

$$0.6\times 10^{-16} \leqslant \sigma_{\mathrm{expt}}^{\mathrm{AI}}(\mathrm{cell}, T=650\ \mathrm{K}) \leqslant 1.4\times 10^{-16}\ \mathrm{cm}^2,$$

where the data of Ref. [2] have been corrected by a factor of 2 according to Ref. [37]. The error bar in the theoretical cross section is estimated by considering the extrapolation procedure of the data for the molecular autoionization cross sections $\sigma^{\mathrm{MA}}(\mathcal{D}pi;\varepsilon)$, beyond the upper value $v_{\mathrm{sup}} = 1750$ m/s for the velocity. Indeed, the Maxwell-Boltzmann collision velocity distribution has a weak, but not vanishing, tail for $v_c > v_{\mathrm{sup}}$, as seen in Appendix B. Whereas the contribution from the velocity range below 1750 m/s leads to a cross section of 1.03×10^{-16} cm^2, the extrapolation procedure introduces an uncertainty in the computed result well below 10%.

The relative contribution of the various molecular autoionization channels to the total cross section is analyzed in Fig. 3. It is manifested that the dominant contribution (40%) comes from the $^3\Pi_u$ channel. Calculations with a transmission coefficient w equal to unity would lead to a too large value of the cross section [(i), Fig. 3(a)]. Neglecting the $^3\Pi_u$ contribution would lead to a cross section of 0.65×10^{-16} cm^2, at the lower limit of the experimental error bar: the agreement between theory and experiment seems better when the $^3\Pi_u$ channel is considered. However, neglecting the $^1\Pi_u$ channel yields a cross section which is still within the experimental error bar [(iv), Fig. 3(a)]. The contribution of the $^3\Sigma_u^+$ channel leads to a cross section of 0.23×10^{-16} cm^2 if α_T is assumed to be 37°, or 0.21×10^{-16} cm^2 with $\alpha_T = 63°$, so that the model of the unique $^3\Sigma_u^+$ channel is ruled out by comparison with this experiment.

The long-range population loss that we have considered for the $^3\Pi_u$ symmetry is also justified *a posteriori* by the agreement between computed and measured cross sections: if all the population of the $(3p+3p)$ asymptote was transferred into the inner region for the $^3\Pi_u$ symmetry, the total cross section would be 1.40×10^{-16} cm^2, at the upper limit of the experimental error bar.

B. Comparison with the Utrecht experiments

As in previous work, our results for the relative variation of the ion signal as a function of the polarization angle θ are in good agreement with the counterpropagating-beam experiments in the 910–1600-m/s velocity range. In Fig. 4 we present, for various values of the average collision velocity $\overline{v_c}$ and different excitation schemes $[\widetilde{a}_A,\widetilde{a}_B]$, a comparison between experimental results and calculations. First, we assume a mixing angle α_T of 37° (*ab initio* value) for the two long-range components of the $^3\Sigma_u^+$ channel. For linear polarization, with the $\mathrm{lin}(+\theta,\pm\theta)$ excitation scheme [Figs. 4(a)–4(c)], the disagreement between theory and experiment is at most 20%. Suppressing the $^3\Pi_u$ channel does not modify the shape of the curve very much. Moreover, in the latter conditions, the agreement with experiment can be markedly improved by varying the mixing angle from 37° to 63°. These results can be analyzed by considering the mo-

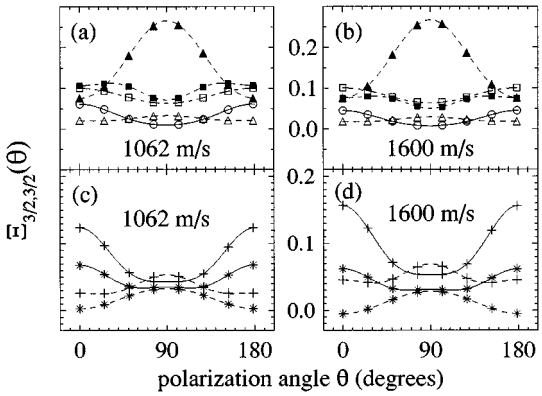

FIG. 5. Molecular weights $\Xi_{3/2,3/2}(\mathcal{D}pi;\widetilde{\alpha}_A\widetilde{\alpha}_B;\overline{v_c})$ [abbreviated as $\Xi_{3/2,3/2}(\theta)$] as a function of the polarization angle θ, for the counterpropagating-beam experiment [lin$(+\theta,+\theta)$ excitation scheme], with $\overline{v_c}=1062$ and 1600 m/s. (a) and (b) Full triangles $\mathcal{D}1\,{}^3\Delta_u$; full squares $\mathcal{D}1\,{}^3\Pi_u$; open squares $\mathcal{D}1\,{}^1\Pi_u$; open triangles $\mathcal{D}1\,{}^1\Delta_g$; open circles $\mathcal{D}2\,{}^1\Sigma_g^+$. (c) and (d) Contributions to $\mathcal{D}2\,{}^3\Sigma_u^+$ from $\mathcal{A}7\,{}^3\Sigma_u^+$ (plus symbols) and $\mathcal{A}8\,{}^3\Sigma_u^+$ (stars) computed for $\alpha_T=37°$ (dashed line) and $\alpha_T=63°$ (full line).

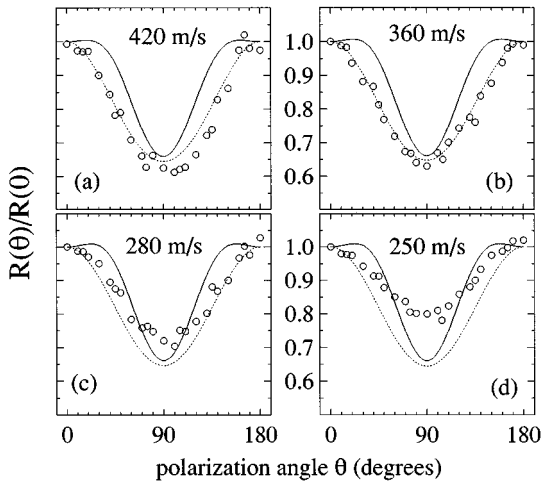

FIG. 6. Associative ionization rate constants $R^{\mathrm{Al}}(\frac{3}{2},\frac{3}{2},\widetilde{\alpha}_A,\widetilde{\alpha}_B,\overline{v_c})$ [abbreviated as $R(\theta)$, and normalized at $\theta=0°$] for a single-beam experiment, as a function of the polarization angle θ in the lin$(+\theta,+\theta)$ excitation scheme, for different values of $\overline{v_c}$. Solid line: all molecular symmetries are considered. Dotted line: all symmetries except $^3\Pi_u$ are considered. Circles: experimental results of the Utrecht group [5].

lecular weights Ξ defined in Eq. (25) and represented in Fig. 5 for the lin$(+\theta,+\theta)$ excitation scheme at two collision velocities, 1062 and 1600 m/s. The absolute value of such coefficients reflects the statistical weight of a given channel [varying from 6 (for $^3\Delta_u$ or $^3\Pi_u$) to 1 (for $^1\Sigma_g^+$)] and can possibly be attenuated by the $w(\mathcal{A}ni\rightarrow\mathcal{D}pi;\varepsilon)$ transmission factor [important in the case of $^3\Pi_u$ symmetry, as displayed in Fig. 2(c)]. Their angular variation is typical of the excitation geometry and of the symmetry of the long-range molecular state. Obviously the θ variation is very similar for the $^3\Pi_u$ and $^1\Pi_u$ channels, and differs markedly for the $^3\Sigma_u^+$ channel; however, the shape of the latter curve can be modified, and even switched from positive to negative contrast, by changing the mixing angle α_T. This is not surprising, as the populations of the $\sigma\sigma$ and $\pi\pi$ long-range components have very different dependences upon the polarization angle. It is then possible to fit the experimental curve at 1062 m/s by suppressing the contribution of the $^3\Pi_u$ and choosing a mixing angle $\alpha_T=63°$. Therefore, the measurements of the *relative* variation cannot be used to discriminate between the Π_u and $^3\Sigma_u^+$ channels, and a more elaborate model of the long-range dynamics should be performed. The presence of the $^3\Delta_u$ channel seems more evident: at 1600 m/s, when this channel is open, it is clear that the *contrast C* is reduced due to its contribution, in agreement with experiment. The curve computed excluding the $^3\Delta_u$'s contribution exhibits a too important contrast.

When the polarization angle is not identical for the two beams, the effect of the $^3\Pi_u$ contribution manifests itself clearly [see Fig. 4(e)]. Nevertheless, this contribution can be partially compensated for by switching the mixing angle, and it is striking that the same empirical value $\alpha_T=63°$ can fit most of the experimental data.

However, as illustrated in Fig. 4(f), at a collision velocity of 910 m/s, and for the [lin(θ),cir$^+(90)$] excitation scheme, suppressing the $^3\Pi_u$ contribution enhances the disagreement between theory and experiment, and switching the mixing angle to $\alpha_T=63°$ causes even stronger disagreement. This can be interpreted from the analysis of the corresponding Ξ coefficients, not represented in the present paper, by remarking that the contrast is much smaller for the $^3\Pi_u$ ionization channel, and it is difficult to interpret the experimental data without including the contribution of this symmetry. Such a result indicates that circular polarization experiments should probably be more sensitive to the presence of a $^3\Pi_u$ channel. We shall further discuss this point below by considering not only relative but also absolute measurements.

An opposite conclusion can be formulated when going to low collision energies. Indeed, considering single-beam experiments [5], where the collision energy is reduced by a factor of 2–8, it seems at first [for $\overline{v_c}=420$, and 360 m/s, see Figs. 6(a) and 6(b)] that the agreement between theory and experiment is improved when the contribution of $^3\Pi_u$, which is markedly peaked around $\theta=90°$, is suppressed. At such energies, switching the mixing between the two $^3\Sigma_u^+$ long-range components does not change the shape of the curve. The decrease of the contribution of the $^3\Pi_u$ channel is coherent with the breakdown of sudden approximation at low collision energies, the Hund's case *c* correlation scheme between a $^3\Pi_u$ intermediate range curve and the two $(3p\,{}^2P_{1/2}+3p\,{}^2P_{1/2})$ and $(3p\,{}^2P_{1/2}+3p\,{}^2P_{3/2})$ asymptotes becoming more adapted [36]. This point should be confirmed by experiments using D_1 line excitation at low energies. Going to low velocities, the disagreement between theory and experiment should indicate the low-energy limit of our model. The collision energy at 420 m/s is 10.5 meV, which is only a factor of 5 larger than the fine-structure splitting of one sodium atom ($\Delta E_{\mathrm{FS}}\approx 17.19\ \mathrm{cm}^{-1}$, or 2.13 meV): the agreement between our calculations and experiments therefore seem surprisingly good. At even lower velocities (250 and 280 m/s) the collision energy exceeds the fine-structure splitting by a factor of 2 only, and therefore is of the same order of magnitude as the sum of the fine-structure splittings for the two atoms, so that our model becomes too crude for any quantitative interpretation.

TABLE IV. Schematic description of the published experimental works studying associative ionization in Na_2, considered for comparison of our computations. The correspondence between the different notations for some excitation schemes used by the Utrecht group and the Maryland group is indicated.

Group	Experimental setup	Collision velocity (v_c) distribution (v_c range (m/s))	Polarization of the exciting laser	Excited transition(s) $3s\ ^2S_{1/2} \rightarrow 3p\ ^2P_{3/2}$ $(FM_F) \rightarrow (F'M'_F)$	Excitation scheme	AI cross section (σ_{AI}) (10^{-16} cm^2)	Observations
HG[2]	Cell (650 K)	Maxwell-Boltzmann $T=650$ K (3D, isotropic)	not defined	No hyperfine selection		1.0 ($\pm$37%)	
MA1[6]	CB 90° (773 K)	Selection of narrow velocity class (1200–2200)	σ^+	$(2,+2)\rightarrow(3,+3)$	cir$^+$(90°,90°)	$1.8<\sigma_{AI}<8.0$	Strong velocity dependence
MA2[7]	CB 90° (635 K)	Selection of narrow velocity class (550–2200)	π	$(2,M_F)$ $\rightarrow$ $[(3,M'_F)(70\%),$ $(2,M'_F)(20\%),$ $(1,M'_F)(10\%)]$	lin(0°,0°) or *axial-axial* lin(90°,90°) or *transverse-transverse*		Strong velocity dependence Selectivity in the spatial alignment of the atomic $3p$ orbitals
MA3[8]	CB 90° and SB (773 K)	Selection of narrow velocity class (200–600) (SB) (800–2200) (CB)	σ^+,σ^-	$(2,\pm2)\rightarrow(3,\pm3)$	[cir$^+$(0°),cir$^-$(180°)] or *parallel* spins [cir$^+$(0°),cir$^+$(180°)] or *antiparallel* spins		Selectivity in spins configurations Strong velocity dependence
MA4[9]	SB (773 K)	Selection of narrow velocity class $v_c=12$ m/s	π and σ	$(2,M_F)\rightarrow(3,M'_F)$ and $(1,M_F)\rightarrow(2,M'_F)$	Excitation geometry not precisely defined for π polarization cir$^+$(225°,45°)	5.1 ± 2.0 (σ) 10.2 ± 4.5 (π)	Polarization dependence
MA5[10]	SB (773 K)	Selection of narrow velocity class (100–625)	π and σ	$(2,\pm2)\rightarrow(3,\pm3)$ (σ) $(2,M_F)$ $(3,-2,\ldots,2)$ (π)	[cir$^+$(45°),cir$^-$(135°)] [cir$^+$(45°),cir$^+$(135°)]		Polarization and excitation geometry dependence Velocity dependence
UT1 [3]	CB 180° (635 K, 575 K)	large profile (width$\geqslant$250 m/s) (900–2300)	π	$(2,M_F)\rightarrow(3,M'_F)$	lin($+\theta,+\theta$)	$0.8\begin{pmatrix}+1.2\\-0.5\end{pmatrix}$	Selectivity of the process with respect to the preparation of the collision partners in magnetic substates ($\overline{\sigma}_{\lvert m_1\rvert,\lvert m_2\rvert}$)

TABLE IV. (Continued).

UT2 [4]	CB 180° (635 K, 575 K)	large profile (width≥250 m/s) (900–2300)	π and σ	$(2,M_F)\rightarrow(3,M_F')$	$\mathrm{lin}(+\theta,+\theta)$	Same properties as UT1
					$\mathrm{lin}(+\theta,-\theta)$	Coherence contributions
					$\mathrm{lin}(+\theta,0°)$	Velocity dependence of some coherence terms
					$\mathrm{lin}(+\theta,90°)$	
					$\mathrm{cir}^{+}(90°,90°)$	
					$\mathrm{cir}^{-}(90°,90°)$	
					$[\mathrm{cir}^{+}(90°),\mathrm{cir}^{-}(90°)]$	
					$[\mathrm{lin}(+\theta),\mathrm{cir}^{+}(90°)]$	
UT3 [5]	SB (575 K)	large profile (width>350 m/s) (100–700)	π and σ	$(2,M_F)\rightarrow(3,M_F')$	$\mathrm{lin}(+\theta,+\theta)$	Polarization and velocity dependence. Quantitative estimation of some coherence terms

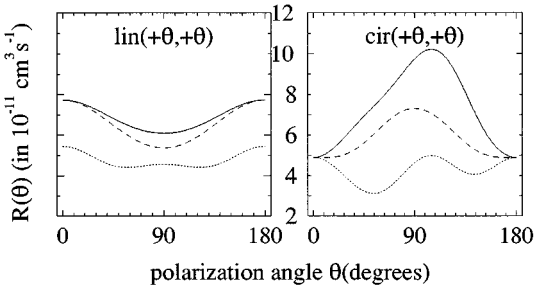

FIG. 7. Computed associative ionization rate $R^{\mathrm{Al}}(\frac{3}{2},\frac{3}{2},\widetilde{\alpha}_A,\widetilde{\alpha}_B,\overline{v_c})$ [abbreviated as $R(\theta)$] as a function of the polarization angle θ, at $\overline{v_c}=1600$ m/s (counterpropagating-beam setup) and for $\alpha_T=37°$. (a) $\mathrm{lin}(+\theta,+\theta)$. (b) $\mathrm{cir}^{+}(+\theta,+\theta)$. Dashed line: including only the diagonal contribution of Eq. (14); solid line: including also all *coherence* terms of Eq. (15); dotted line: idem, excluding the $^3\Pi_u$ channel.

The previous discussion was considering only relative variation of the ion signal. It is important to recall that the ion rate is substantially lowered when the contribution of the $^3\Pi_u$ channel is not included. This is illustrated in Fig. 7, where we have represented the predicted ion signal at a collision velocity of 1600 m/s, in the hypothesis of two counterpropagating beams and for two excitation schemes, lin $(+\theta,+\theta)$ as in Fig. 4(b) and $\mathrm{cir}^{+}(+\theta,+\theta)$. The latter excitation scheme was never studied experimentally. We discuss through these two schemes the contribution of the $^3\Pi_u$ autoionization channel and of the effects of the coherence terms. In the $\mathrm{lin}(+\theta,+\theta)$ excitation scheme, it is manifested that when the $^3\Pi_u$ contribution is neglected, the absolute value of the signal is decreased by 40%, the contrast being reduced. In the $\mathrm{cir}^{+}(+\theta,+\theta)$ excitation scheme, not only the intensity of the signal but the shape of its θ dependence is very much modified when this contribution is neglected. The effect of coherences is also much stronger for circular polarization. We therefore suggest that such experimental studies could possibly provide deeper insight into the collision mechanism.

A study of the velocity variation of some cross sections has also been performed by the Utrecht group. In Fig. 8 we present the comparison of our calculations with absolute measurements [3–5] of the $\overline{\sigma_{j_A=3/2,|m_A|;j_B=3/2,|m_B|}}$ partial cross sections, hereafter labeled $\overline{\sigma_{|m_A|,|m_B|}}$, and computed as

$$\overline{\sigma_{|m_A|,|m_B|}}=\tfrac{1}{2}(\sigma_{m_A m_B}+\sigma_{m_A,-m_B}), \tag{29}$$

as well as σ_{iso} defined as

$$\sigma_{\mathrm{iso}}=\tfrac{1}{4}(\overline{\sigma_{3/2,3/2}}+2\overline{\sigma_{3/2,1/2}}+\overline{\sigma_{1/2,1/2}}). \tag{30}$$

In Eq. (29), the cross sections written in simplified notations $\sigma_{m_A m_B}$ are defined by Eq. (14) with $j_A=j_B=\frac{3}{2}$. The experimental cross sections have been velocity deconvoluted, and are reported here in absolute values according to the calibration suggested by the authors of Ref. [4], that is 100 arb. units$=10^{-16}$ cm^2 (with a factor of 2 of uncertainty) for the cross sections $\overline{\sigma_{|m_A|,|m_B|}}$ as well as for σ_{iso}. The agreement with experimental results seems satisfactory for σ_{iso} [see Fig. 8(d)] and $\overline{\sigma_{3/2,1/2}}$ [see Fig. 8(b)], where an analysis of the calculations shows that many symmetries

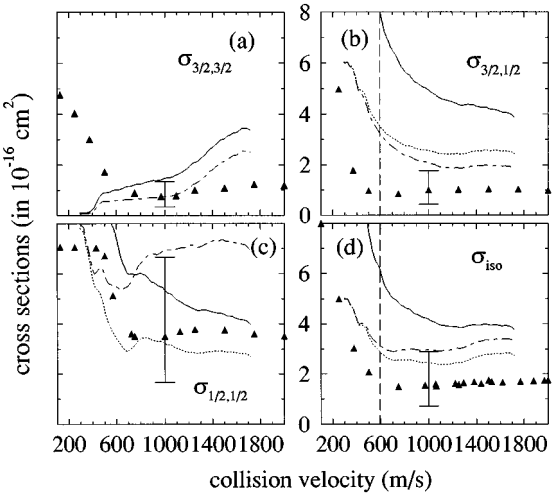

FIG. 8. Absolute associative ionization (partial) cross sections $\overline{\sigma_{|m_A|,|m_B|}}$, and isotropic cross section $\sigma_{\rm iso}$ as a function of the collision velocity v_c, compared to the experimental results of the Utrecht group [3,4,5]. Solid line: including all symmetries, and $\alpha_T = 37°$. Dotted line: including all symmetries except $^3\Pi_u$, and $\alpha_T = 37°$. Dot-dashed line: including all symmetries except $^3\Pi_u$, and $\alpha_T = 63°$. Full triangles: experiment. The dashed line figures the low velocity validity range of our model. The error bar represents the experimental error (by a factor of 2) in the scaling of the absolute cross sections (see Ref. [4]).

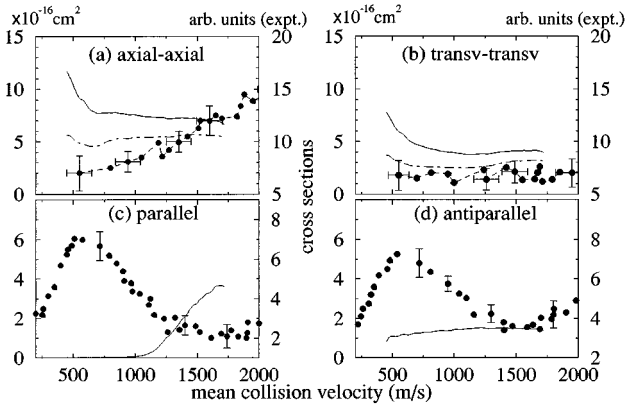

FIG. 9. Associative ionization cross sections as a function of the collision velocity v_c, compared to the crossed-beam experimental results of the Maryland group [7,8], computed with $a_T = 63°$, for different excitation schemes: (a) axial-axial [or lin(0°,0°)]; (b) transverse-transverse [or lin(90°,90°)]; (c) circular polarization with [cir$^+$(0°),cir$^-$(180°)] or parallel spin configuration; (d) with [cir$^+$(0°),cir$^+$(180°)] or antiparallel spin configuration. Solid line: including all symmetries; dot-dashed line: including all symmetries except $^3\Pi_u$; full circles: experiment. Note that in the excitation schemes displayed in (c) and (d) the $^3\Pi_u$ channel is not efficient. An absolute scale is used for the computed results, and the experimental scale (in arbitrary units) is shifted to fit the order of magnitude of our results.

contribute to the cross section. For $\overline{\sigma_{3/2,3/2}}$ the long-range adiabatic curves that may be populated are exclusively $^3\Delta_u$, $^3\Sigma_u^+(\pi\pi)$, and $^1\Sigma_g^+(\pi\pi)$. We interpret the rise of the theoretical cross section [see Fig. 8(a)] at higher energies as the opening of a $^3\Delta_u$ autoionization channel, and this effect is not clearly manifested in the experimental signal. At lower collision energies, the decrease of the theoretical cross section comes from the vanishing of the $w(\mathcal{A}ni \rightarrow \mathcal{D}pi;\varepsilon)$ transmission factor [see Fig. 2(c)] due to a hump in the $8\,^3\Sigma_u^+$ long-range curve, together with a decrease of the autoionization efficiency for the $\mathcal{A}7\,^3\Sigma_u^+$ long-range curve [see Fig. 2(b)]. This is apparently in contradiction to the rise in the experimental curve. However, as discussed earlier, our model is certainly not valid when the collision energy becomes of the same order of magnitude as the fine-structure splitting of the set of two sodium atoms, and from the present discussion we can estimate the lower limit for the validity of our model at velocities around 600 m/s $[\varepsilon/(2\Delta E_{\rm FS}) \approx 5]$. The rise in the experimental curve would be compatible with a breakdown of sudden approximation for spin uncoupling, leading to population of either $^1\Pi_u$ or $^3\Pi_u$ autoionization channels, for which the cross section increases at low collision energies [see Fig. 2(b)]. In the same way, we see in Fig. 8(c) that the shape of the computed cross section $\overline{\sigma_{1/2,1/2}}$ markedly depends upon the inclusion of the $^3\Pi_u$ autoionization channel and upon the choice for the mixing angle α_T between the two long-range components of the $^3\Sigma_u^+$ channel. However, it is not possible to use the experimental data to discriminate the various hypotheses, as once again the low-energy rise in the measured cross section occurs in a region where the fine-structure effects should be considered within a model more elaborate than ours.

C. Comparison with the Maryland experiments

A comparison of the velocity dependence of our calculated cross sections with the measurements performed in Maryland [7,8] is displayed in Fig. 9. The experimental data given in arbitrary units are scaled there in such a manner that they appear in the same zones of the computed results. The theoretical cross sections are computed according to Eq. (21), with atomic density matrices corresponding to the following excitation schemes: lin(0,0) [denoted by axial-axial, Fig. 9(a)], lin(90,90) [or transverse-transverse, Fig. 9(b)], $\lfloor$cir$^+$(0),cir$^-$(180)$\rfloor$ [producing a parallel spin configuration, Fig. 9(c)] and $\lfloor$cir$^+$(0),cir$^+$(180)$\rfloor$ [giving rise to an antiparallel spins configuration, Fig. 9(d)]. For two excitation schemes, the computed results agree reasonably with the experimental ones [Figs. 9(a) and 9(b)]. In particular, an important aspect of the observations is reproduced: the scheme axial-axial is more in favor than the transverse-transverse one to the ionization process. Suppressing the $^3\Pi_u$ contribution seems to improve the agreement at low collision velocities in the first excitation scheme.

In contrast, there is disagreement between our calculations and the experimental results for the two schemes parallel and antiparallel presented in Figs. 9(c) and 9(d). First, the rise of the theoretical cross section, due to the opening of the $^3\Delta_u$ channel, at around 70 meV, corresponding to a collision velocity of 1000 m/s, is not observed experimentally [Fig. 9(c)]. Second, our present model does not explain the peak in the experimental curve observed below 500 m/s. In fact, since in our model $^3\Delta_u$ is the unique channel populated by the parallel scheme, the cross section in Fig. 9(c) is directly proportional to the molecular autoionization cross section of this state, plotted in Fig. 2(b). Moreover, the antiparallel excitation scheme only populates the $^3\Sigma_u^+$ and $^1\Sigma_g^+$

channels, and we can see in Fig. 2(b) that the combined autoionization cross section of the $\mathcal{A}7$ and $\mathcal{A}8$ states of the former symmetry, as well as the cross section of latter one, is nearly constant for $\varepsilon > 14$ meV ($v_c > 500$ m/s). This explains the flat shape of the theoretical curve of Fig. 9(d).

In the Utrecht experiments discussed above and reported in Fig. 8, there was an increase of the cross section at low velocities, but no peak occured. So the two sets of experimental results also appear to disagree. It would therefore be valuable that more experimental and theoretical works give deeper insight into the collision mechanism at low energies.

V. CONCLUSION

Being a simple example of the formation of a chemical bond, the associative ionization reaction between two excited sodium atoms has been the subject of many experimental and theoretical efforts [1]. However, up to now there has been little confrontation between theory and experiment. The aim of the present paper therefore has been to check the most complete existing theoretical models with experimental results for the total cross section and for the polarization and velocity dependence of the Na_2^+ ion signal.

The difficulty in the theoretical treatment comes from the large number of molecular symmetries that are involved in the process, and from the matching at intermediate distances of two very different dynamical problems. At short internuclear distances we have used previous MQDT calculations [18,20] to describe the autoionization of the Na_2 molecule via $^3\Sigma_u^+$, $^1\Sigma_g^+$, $^3\Pi_u$, $^1\Pi_u$, and $^1\Delta_g$ channels, and we have performed calculations for the $^3\Delta_u$ channel, through which the autoionization process can only occur for collision energies above a threshold of 70 meV. In order to estimate the population of these six short-range doubly excited autoionizing states from two separated atoms, we have proposed a simple model. The main hypotheses are smooth connection between short-range molecular diabatic curves and long-range adiabatic curves, and a simple evaluation of the population of states corresponding to such potential curves by considering infinite locking radius, sudden decoupling of the spin at infinite internuclear distances, and, finally, an approximate treatment of population sharing between molecular states at large distances. This treatment allows for the mixing of the two $\sigma\sigma$ and $\pi\pi$ components of the $^3\Sigma_u^+$ and $^1\Sigma_g^+$ long-range states, and the population loss at the various pseudocrossings due to the ionic-covalent interaction. The latter phenomenon, treated in the framework of a very simple Landau-Zener model, is mainly reducing the population transfer to the $^3\Pi_u$ short-range autoionizing state, especially at large collision energies. The model developed in this paper takes into account the coherence effects, as in previous theoretical treaments [14,15]. But, for the first time, to our knowledge, a quantitative evaluation is proposed for the contribution of the coherence terms to the total cross section or to the rate constant of associative ionization process. The originality of the present work is to propose computed values for the cross sections from the contributions of various molecular symmetries, combining short- and long-range dynamics.

Our results seem in good agreement with the total cross section measured by Huennekens and Gallagher in a cell experiment at 650 K. The $^3\Pi_u$ symmetry contributes to half the cross section, and there is an important contribution of the $^1\Pi_u$ channel, so that the model of a unique $^3\Sigma_u^+$ autoionizing channel seems to be unrealistic.

Good agreement is also obtained with the polarization measurements of the Utrecht group, at least for collision velocities $v_c > 400$ m/s ($\varepsilon > 9$ meV). We show that, due to the existence of several autoionizing channels, relative measurements of the variation of the ion signal as a function of the polarization angle cannot be used as a definite proof for the identification of the symmetry of the molecular doubly excited states which are present. For instance, in schemes using linear polarization, the contribution of the $^3\Pi_u$ channel can be compensated for by varying the mixing angle between the two $\sigma\sigma$ and $\pi\pi$ asymptotic contributions to the $^3\Sigma_u^+$ channel. However, absolute measurements, or measurements using circular polarization, are more sensitive to the presence of a Π_u channel, and we suggest that complementary measurements could check this point.

Our results also seem in satisfactory agreement with the velocity-dependent cross sections experimentally deduced by the Utrecht group through a velocity-deconvolution procedure. Some disagreements at velocities below 600 m/s ($\varepsilon < 21$ meV) can easily be attributed to the breakdown of the model of sudden spin uncoupling. Indeed, a proper treatment of long-range dynamics including fine-structure coupling should be introduced in the model below collision energies of 21 meV.

Finally, some disagreement is present with the measurements of the Maryland group [6,8] for the velocity dependence of the cross sections. Such measurements were performed with a narrow velocity distribution, so that no convolution procedure has to be introduced in the comparison between calculated and experimental cross sections. Whereas the theoretical and measured curves look similar in the case of a linear polarization scheme, the maximum observed in the experiment when the atoms are excited with circularly polarized light cannot easily be explained. The breakdown of our model for long-range dynamics below 500 m/s could be one reason, but the experimental cross section displays an energy variation different from the flat theoretical one at velocities well above this value.

In conclusion, for experiments with two perpendicular crossed atomic beams excited by circularly polarized lasers, the presence of a sharp minimum in the energy variation of the cross section should be confirmed. A physical interpretation should be developed: as the autoionization cross sections for the various symmetries are slowly varying functions of the collision energy, the model for the population transfer from two atoms to a doubly excited autoionizing curve should be reconsidered. They were very approximately estimated in the present work, by means of a semiclassical Landau-Zener model allowing for population loss from one adiabatic curve to another one of the same symmetry. No coupling between curves of different symmetries is included. Close-coupling calculations at long range should be performed, considering rotational coupling effects. At low collision energies, such calculations should take fine-structure effects into account. In all cases, those calculations should be connected to a short-range MQDT treatment of the autoionization process, which is not an easy task.

Nevertheless, the present work seems to show a satisfactory agreement, at collision energies where a sudden uncoupling of the spin is a realistic hypothesis, between most experimental data for associative ionization between two Na($3p$) atoms and a theoretical model where the contributions of $^3\Sigma_u^+$, $^1\Sigma_g^+$, $^3\Pi_u$, $^1\Pi_u$, $^1\Delta_g$, and $^3\Delta_u$ channels are considered for the autoionization of the molecule formed during the collision. A more precise check of the contribution of those channels is considered in a work in progress, where theory is confronted to experiments analyzing the vibrational distribution of the product ions [38].

APPENDIX A: CALCULATION OF THE COEFFICIENTS w FOR POPULATION TRANSFER

We use the semiclassical model developed in Ref. [28], which is simplified in the present problem, since for each symmetry only one pseudocrossing occurs. Let us consider a collision with energy ε and impact parameter b, where the population of the adiabatic molecular state $\mathcal{A}ni$ is $\mathcal{N}(\mathcal{A}ni;\varepsilon,b)$ at large internuclear distances. As discussed in Ref. [28], the adiabatic curves of $^3\Pi_u$ and $^3\Sigma_u^+$ symmetries exhibit at $R_c=26a_0$ and $23.2a_0$, respectively, an avoided crossing with a neighboring curve of the same symmetry ($\mathcal{A}n'i$) correlated to Na($3s$)+Na($4d$), while for the $^1\Delta_g$ symmetry the equivalent avoided crossing occurs at $R_c=15.1a_0$. We estimate that, for $R<R_c$, the population of the adiabatic curve is

$$\mathcal{N}'(\mathcal{A}ni;\varepsilon,b)=\mathcal{N}(\mathcal{A}ni;\varepsilon,b)[1-\mathcal{P}_{\mathrm{LZ}}(\varepsilon,b;\mathcal{A}ni\rightarrow\mathcal{A}n'i)], \tag{A1}$$

where $\mathcal{P}_{\mathrm{LZ}}$ is the Landau-Zener probability for population transfer to the $\mathcal{A}n'i$ curve at the pseudocrossing. We checked that the ratio $\mathcal{N}'/\mathcal{N}$ does not vary significantly as a function of b in the range of impact parameters considered in the present problem. We therefore simply compute the population transfer coefficient as an average value over partial waves, the $\mathcal{A}ni$ curve being correlated to the short-range diabatic curve $\mathcal{D}pi$:

$$w(\mathcal{A}ni\rightarrow\mathcal{D}pi;\varepsilon)=\frac{1}{L_{\max}}\sum_{L=0}^{L_{\max}}[1-\mathcal{P}_{\mathrm{LZ}}(\varepsilon,L;\mathcal{A}ni\rightarrow\mathcal{A}n'i)], \tag{A2}$$

where the correspondence between impact parameter b and partial wave L is $b\sqrt{2\mu\varepsilon}=\sqrt{L(L+1)}$, and $L_{\max}$ is the maximum partial wave for which autoionization may take place.

In the present calculations, $L_{\max}$ varies from 29 to 132 when the energy ε increases from 1 to 184 meV, corresponding to a range of variation of b from 0 to $23.8a_0$ at 1 meV and from 0 to $7.9a_0$ at 184 meV. The Landau-Zener probability varies by no more than 14% in the range 0–132 of L, justifying the use of a mean transmission coefficient instead of a quantity depending upon the partial wave.

In the case of the $^1\Sigma_g^+$ symmetry, there is an avoided crossing at $R_c=15.25a_0$ between the $7i$ and the $8i$ potential curves, so that

$$w(\mathcal{A}8i\rightarrow\mathcal{D}2i;\varepsilon)=\frac{1}{L_{\max}}\sum_{l=0}^{L_{\max}}[1-\mathcal{P}_{\mathrm{LZ}}(\varepsilon,L;\mathcal{A}8i\rightarrow\mathcal{A}7i)], \tag{A3}$$

with $L_{\max}=229$ and for $\varepsilon>30$ meV. For $\varepsilon<30$ meV, due to a hump in the $8i$ potential curve, no flux is transmitted to the inner region.

In the case of the $^3\Sigma_u^+$ symmetry, two avoided crossings very close to each other occur at $R_c=23.16a_0$ and $R_c=23.00a_0$ between the $\mathcal{A}8i$ and $\mathcal{A}9i$ potential curves, and between the $\mathcal{A}8i$ and the $\mathcal{A}7i$ potential curves, respectively. As in Ref. [28], we consider these two pseudocrossings as independent, which yields only crude estimations in the following calculations. Therefore, as the $\mathcal{A}7i$ curve is correlated to the $\mathcal{D}1i$ doubly excited state, which does not contribute to the autoionization process, we write

$$w(\mathcal{A}7i\rightarrow\mathcal{D}2i;\varepsilon)=\frac{1}{L_{\max}}\sum_{L=0}^{L_{\max}}[\mathcal{P}_{\mathrm{LZ}}(\varepsilon,L;\mathcal{A}8i\rightarrow\mathcal{A}7i)], \tag{A4}$$

$$w(\mathcal{A}8i\rightarrow\mathcal{D}2i;\varepsilon)=\frac{1}{L_{\max}}\sum_{L=0}^{L_{\max}}[1-\mathcal{P}_{\mathrm{LZ}}(\varepsilon,L;\mathcal{A}8i\rightarrow\mathcal{A}7i)]\times[1-\mathcal{P}_{\mathrm{LZ}}(\varepsilon,b;\mathcal{A}8i\rightarrow\mathcal{A}9i)]. \tag{A5}$$

As the coupling between the $\mathcal{A}8i$ and $\mathcal{A}9i$ curves is weak, the condition

$$w(\mathcal{A}7i\rightarrow\mathcal{D}2i;\varepsilon)+w(\mathcal{A}8i\rightarrow\mathcal{D}2i;\varepsilon)=1$$

is nearly fullfilled, so that in our model population of both $\mathcal{A}7i$ and $\mathcal{A}8i$ states will contribute to autoionization.

APPENDIX B: VELOCITY DISTRIBUTIONS

In order to reproduce with our model the experimental results of the AI reaction, we need to know the collision velocity distributions corresponding to each experimental setup with which we are concerned.

1. Distribution of atomic velocities

In a medium in thermal equilibrium at temperature T_e, the number of atoms of mass m_a moving with a velocity lying between $\mathbf{v}$ and $\mathbf{v}+d\mathbf{v}(d\mathbf{v}=v^2dv\ d\Omega)$ is given by the well-known Maxwell-Boltzmann (MB) distribution

$$f^{\mathrm{MB}}(\mathbf{v})d\mathbf{v}=\left(\frac{m_a}{2\pi k_BT_e}\right)^{3/2}\exp\left(-\frac{m_a\mathbf{v}^2}{2k_BT_e}\right)d\mathbf{v}, \tag{B1}$$

where k_B is Boltzmann's constant.

In an isotropic cell ($T_e=T_c$), by integrating over the angular coordinates, one obtains

$$f_0^{\mathrm{MB}}(v)dv=\left(\int d\Omega\ f^{\mathrm{MB}}(\mathbf{v})\right)v^2dv$$
$$=4\pi\left(\frac{m_a}{2\pi k_BT_c}\right)^{3/2}v^2\ \exp\left(-\frac{m_av^2}{2k_bT_c}\right)dv. \tag{B2}$$

For a thermal beam ($T_e=T_b$) directed along an axis $\hat{z}$, the atomic velocity distribution is defined by

$$f_b^{\mathrm{MB}}(v)dv=\left(\int d\Omega\, f^{\mathrm{MB}}(v)\,\delta(\hat{v}-\hat{z})\right)v^2dv$$
$$=\left(\frac{2m_a{}^3}{\pi k_B{}^3T_b{}^3}\right)^{1/2}v^2\ \exp\left(-\frac{m_av^2}{2k_bT_b}\right)h(v)dv, \tag{B3}$$

with

$$h(v)=\begin{cases}1, & v>0\\ 0, & v<0.\end{cases}$$

2. Distribution of relative velocities

The distribution of magnitudes of the relative collision velocity v_c for a cell is defined by

$$f_{\mathrm{cell}}(v_c)=\int d\mathbf{v}_1\int d\mathbf{v}_2 f^{\mathrm{MB}}(\mathbf{v}_1)f^{\mathrm{MB}}(\mathbf{v}_2)\,\delta(v_c-|\mathbf{v}_1-\mathbf{v}_2|) \tag{B4}$$

$$=\frac{4}{\sqrt{\pi}}\left(\frac{m_a}{4k_BT_c}\right)^{3/2}v_c{}^2\ \exp\left(-\frac{m_av_c{}^2}{4k_BT_c}\right). \tag{B5}$$

This function of v_c is plotted in Fig. 10(a).

For collisions between atoms within a single beam (T_b) and from two different beams with the respective temperatures T_{b1} and T_{b2}, the collision velocity distribution has the following expression:

$$F_{\mathrm{G}}(v_c)=\int_0^\infty dv_1\int_0^\infty dv_2 f_{b1}^{\mathrm{MB}}(v_1)f_{b2}^{\mathrm{MB}}(v_2)$$
$$\times\delta[v_c^2-\beta(v_1,v_2)], \tag{B6}$$

where

$$\beta(v_1,v_2)=v_1^2+v_2^2-2v_1v_2\ \cos(\mathbf{v}_1,\mathbf{v}_2),$$
$$\mathrm{G}=\mathrm{SB},\ \mathrm{CB180°},\ \mathrm{CB90°}.$$

For single-beam (SB) and counterpropagating-beam (CB180°) geometries, $\cos(\mathbf{v}_1,\mathbf{v}_2)$ equals plus or minus unity, respectively, and vanishes obviously for orthogonal crossed-beam (CB90°) geometry. In the latter case, Eq. (B6) can be integrated analytically:

$$F_{\mathrm{CB90°}}(v_c)=\left(\frac{m_a}{2k_BT_b}\right)^3v_c{}^5\ \exp\left(-\frac{m_av_c{}^2}{2k_BT_b}\right). \tag{B7}$$

For the SB and CB180° geometries, the integration in Eq. (B6) cannot be easily achieved in an analytical way. However, a complicated analytical expression of $F_{\mathrm{SB}}(v_c)$ can be found in Ref. [39], while $F_{\mathrm{CB180°}}(v_c)$ has never been written analytically. The three functions $F_{\mathrm{XG}}(v_c)$, G=SB, CB180°, CB90°, [Eq. (B6)] are also displayed in Fig. 10(a). The analytical expression (B7) is used for the CB90° geometry, while numerical integrations have to be performed for the SB and CB180° experimental setups.

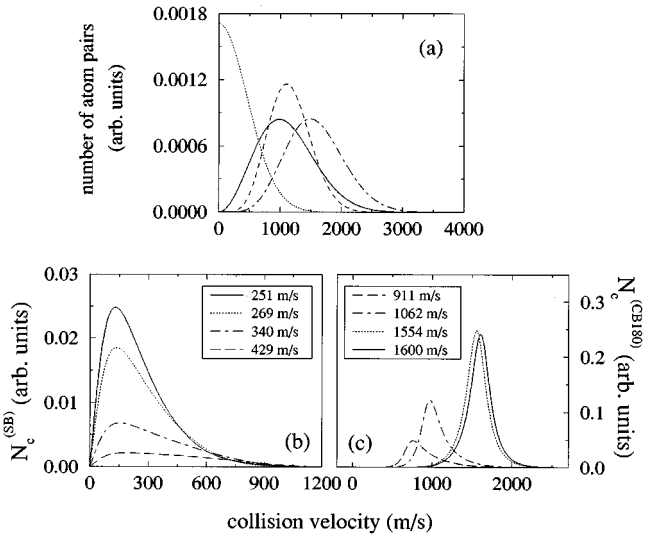

FIG. 10. Distributions of collision velocities. (a) Normalized distributions without velocity selection, at temperature $T_e=T_c=T_b=650$ K. Solid line: cell; dot-dashed line: counterpropagating beams; dashed line: orthogonally crossed beams: dotted line: single beam. (b) and (c) The numbers of collisions $N_c^{(XG)}(v_c)$ at $T_b=575$ K for different laser detunings $\delta\nu_L$ corresponding to different averaged collision velocities $\overline{v_c}$ (see text). (b) Single-beam geometry. Solid line: $\delta\nu_L=57$ MHz or $\overline{v_c}=251$ m/s; dotted line: $\delta\nu_L=75$ MHz or $\overline{v_c}=269$ m/s; dot-dashed line: 95 MHz or $\overline{v_c}=340$ m/s, long-dashed line: $\delta\nu_L=110$ MHz or $\overline{v_c}=429$ m/s. (c) Counterpropagating-beam geometry. Long-dashed line: $\delta\nu_L=31$ MHz or $\overline{v_c}=911$ m/s; dot-dashed line: $\delta\nu_L=41$ MHz or $\overline{v_c}=1062$ m/s; dotted line: $\delta\nu_L=68$ MHz or $\overline{v_c}=1554$ m/s, solid line: $\delta\nu_L=70$ MHz or $\overline{v_c}=1600$ m/s.

3. Velocity selection by Doppler effect

With a laser of frequency ν_L, propagating along the direction $\mathbf{u}_L$, one excites a transition with frequency ν_0 (value corresponding to atoms at rest) of atoms moving with a velocity $\mathbf{v}=\mathbf{v}_0$, such that

$$\nu_0=\nu_L\left(1+\frac{\mathbf{v}_0\cdot\mathbf{u}_L}{c}\right)=\nu_L\left(1+\frac{v_0\ \cos\ \alpha}{c}\right), \tag{B8}$$

where α is the angle $(\mathbf{v}_0,\mathbf{u}_L)$, and v_0 the magnitude of $\mathbf{v}_0$.

In a cell, the angle α in Eq. (B8) is randomly distributed because of the isotropic motion of the atoms. Therefore, for an incident frequency v_L approaching v_0, one excites all atoms of the Maxwell-Boltzmann profile $f_0^{\mathrm{MB}}(v)$ without selecting them in velocities.

In atomic beams experiments, the geometry fixes the direction of the atomic velocity $\mathbf{v}$: for a given direction $\mathbf{u}_L$ of the laser (α fixed), one selects one group of atoms of velocity v_0, given by Eq. (B8). This velocity class has a finite width,

corresponding to the width of the atomic transition. The velocity distribution of excited atoms is defined in literature by multiplying the function $f_b^{\mathrm{MB}}(v)$, given by Eq. (B3), by the probability $A(v;v_0,\alpha)$ of exciting an atom of velocity v ''close to v_0:''

$$f_b^*(v;v_0,\alpha)=A(v;v_0,\alpha)f_b^{\mathrm{MB}}(v). \tag{B9}$$

The probability $A(v;v_0,\alpha)$ (absorption profile) is generally a Lorentzian function of the variable $(v-v_0)$ with a width given by the saturation width $(\Delta\nu_S)$ of the atomic excited level broadened by the exciting power.

For collisions between velocity-selected atoms, we follow the procedure of Ref. [5] in defining the distribution of collision velocities in a way appropriate to collision processes. This consists in defining the distribution function as the number of collisions per unit of interaction volume, unit of time and unit cross section:

$$N_c^{(\mathrm{G})}(v_c)=Pv_cF_{\mathrm{XG}}^*(v_c), \tag{B10}$$

$F_{\mathrm{G}}^*(v_c)$ is given by Eq. (B6), but in which the functions $f_b^*(v_i)$ [Eq. (B9)], must be substituted for the previous ones $f_b^{\mathrm{MB}}(v_i)$. As noted in Ref. [37], the statistical factor P must be introduced to count rigorously the collisions: $P=\frac{1}{2}$ for the case of identical interacting atoms belonging to a same beam or emerging from two beams having a common temperature, and $P=1$ otherwise. The integration is now impossible analytically for all the three-beam experiment geometries we have considered, because of the presence of the factor $A(v;v_0,\alpha)$.

Considering the atomic transition

$$[3s;^2S_{1/2}(F=2)]\rightarrow[3p;^2P_{3/2}(F=3)],$$

which is excited in most experiments and using the expression of the Utrecht group [3] for the probability function

$$A(\nu_0-\nu_L,v)=\left\{1+4\left[\frac{\nu_0-\nu_L+\nu_L\left(\frac{v}{c}\right)\cos\alpha}{\Delta\nu_S}\right]^2\right\}^{-1} \tag{B11}$$

of the laser detuning $\delta\nu_L=\nu_0-\nu_L$, written equivalently in a (non-normalized) Lorentzian form by virtue of Eq. (B8):

$$A(v;v_0,\alpha)=\frac{[(\Delta\nu_S\lambda_L/\cos\alpha)/2]^2}{(v-v_0)^2+[(\Delta\nu_S\lambda_L/\cos\alpha)/2]^2} \tag{B12}$$

(λ_L is the wavelength of the exciting laser), we have performed numerical calculations for $N_c^{\mathrm{G}}(v_c)$ corresponding to the SB and CB180° geometries. The results for different laser detunings $\delta\nu_L$, resulting in different averaged collision velocities $\mathbf{v}_c$, are displayed in Figs. 10(b) and 10(c). The plots are, as they must be, of the same forms of those presented by the Utrecht group [3,5]. Details concerning the average procedure can be found in Ref. [5].

[1] J. Weiner, F. Masnou-Seeuws, and A. Giusti-Suzor, Adv. At. Mol. Phys. **26**, 209 (1990).

[2] J. Huennekens and A. Gallagher, Phys. Rev. A **28**, 1276 (1983).

[3] H. A. J. Meijer, H. P. van der Meulen, and R. Morgenstern, Z. Phys. D **5**, 299 (1987).

[4] H. A. J. Meijer, T. J. C. Pelgrim, H. G. M. Heideman, R. Morgenstern, and N. Andersen, J. Chem. Phys. **90**, 739 (1989).

[5] H. A. J. Meijer, Z. Phys. D **17**, 257 (1990).

[6] M.-X. Wang, M. S. de Vries, J. Keller, and J. Weiner, Phys. Rev. A **32**, 681 (1985).

[7] M.-X. Wang, J. Keller, J. Boulmer, and J. Weiner, Phys. Rev. A **34**, 4497 (1986).

[8] M.-X. Wang, J. Keller, J. Boulmer, and J. Weiner, Phys. Rev. A **35**, 934 (1987).

[9] H. R. Thorsheim, Y. Wang, and J. Weiner, Phys. Rev. A **41**, 2873 (1990).

[10] Y. Wang and J. Weiner, Phys. Rev. A **42**, 675 (1990).

[11] H. A. J. Meijer, S. Schohl, M. W. Muller, H. Dengel, M.-W. Ruf, and H. Hotop, J. Phys. B **24**, 3621 (1991).

[12] M.-X. Wang and J. Weiner, Phys. Rev. A **39**, 405 (1989).

[13] X. Urbain, J. J. Blangé, H. A. Dijkerman, H. Rudolph, and H. G. M. Heideman, J. Phys. B **27**, L245 (1994).

[14] G. Nienhuis, Phys. Rev. A **26**, 3137 (1982).

[15] D. M. Jones and J. S. Dahler, Phys. Rev. A **35**, 3688 (1987).

[16] S. Geltman, J. Phys. B **21**, L735 (1988).

[17] A. Henriet, O. Dulieu, and F. Masnou-Seeuws, Z. Phys. D **18**, 287 (1991).

[18] O. Dulieu, A. Giusti-Suzor, and F. Masnou-Seeuws, J. Phys. B **24**, 4391 (1991).

[19] S. Magnier, Ph. Millié, O. Dulieu, and F. Masnou-Seeuws, J. Chem. Phys. **98**, 7113 (1993).

[20] O. Dulieu, S. Magnier, and F. Masnou-Seeuws, Z. Phys. D **32**, 229 (1994).

[21] H. R. Thorsheim, J. Weiner, and P. S. Julienne, Phys. Rev. Lett. **58**, 2420 (1987).

[22] L. P. Ratliff, M. E. Waghsul, P. D. Lett, S. L. Rolston, and W. D. Phillips, J. Chem. Phys. **101**, 2638 (1994).

[23] V. Bagnato, L. Marcassa, C. Tsao, Y. Wang, and J. Weiner, Phys. Rev. Lett. **70**, 3225 (1993).

[24] P. A. Molenaar, Ph.D. thesis, Utrecht, 1996; P. A. Molenaar, P. van der Straten, and H. G. M. Heideman, Phys. Rev. Lett. **77**, 1460 (1996).

[25] C. C. Tsao, R. Napolitano, Y. Wang, and J. Weiner, Phys. Rev. A **51**, R18 (1995).

[26] M. Klapisch, Comput. Phys. Commun. **2**, 239 (1971).

[27] S. Magnier, M. Aubert-Frécon, O. Bouty, F. Masnou-Seeuws, Ph. Millié, and V. N. Ostrovsky, J. Phys. B **27**, 1723 (1994).

[28] I. Yu Yurova, O. Dulieu, S. Magnier, F. Masnou-Seeuws, and V. N. Ostrovsky, J. Phys. B **27**, 3659 (1994).

[29] E. E. Nikitin and S. Ya. Umanskii, in *Theory of Slow Atomic Collisions* (Springer, Berlin, 1984).

[30] I. V. Hertel, H. Schmidt, A. Bahring, and E. Meyer, Rep. Prog. Phys. **48**, 375 (1987).

[31] J. Grosser, Z. Phys. D **3**, 39 (1986).

[32] E. I. Dashevskaya and E. E. Nikitin, J. Chem. Soc. Faraday Trans. **89**, 1567 (1993).

[33] E. I. Dashevskaya, F. Masnou-Seeuws, and E. E. Nikitin, J. Phys. B **29**, 395 (1996).
[34] E. I. Dashevskaya, F. Masnou-Seeuws, and E. E. Nikitin, J. Phys. B **29**, 415 (1996).
[35] I. Yu Yurova, J. Phys. B **28**, 999 (1995).
[36] O. Dulieu, S. Magnier, B. Lévy, F. Masnou-Seeuws, and Ph. Millié, Phys. Rev. Lett. **76**, 2858 (1996).
[37] N. N. Bezuglov, A. N. Klucharev, and V. A. Sheverev, J. Phys. B **20**, 2497 (1987).
[38] O. Dulieu, X. Urbain, F. Masnou-Seeuws, and H. Rudolph (unpublished).
[39] W. E. Baylis, Can. J. Phys. **55**, 1924 (1977).